American Journal of Modern Physics
2019; 8(2): 18-36
http://www.sciencepublishinggroup.com/j/ajmp
doi: 10.11648/j.ajmp.20190802.12
ISSN: 2326-8867 (Print); ISSN: 2326-8891 (Online)

Best Performance of n^+ - p Crystalline Silicon Junction Solar Cells at 300 K, Due to the Effects of Heavy Doping and Impurity Size. I

Huynh Van Cong*, Paul Blaise*, Olivier Henri-Rousseau

Department of Physics, Laboratory of Mathematics and Physics, University of Perpignan, Perpignan, France

Email address:

huynh@univ-perp.fr (H. V. Cong), huynhvc@outlook.fr (H. V. Cong), blaise@univ-perp.fr (P. Blaise)

*Corresponding author

To cite this article:

Huynh Van Cong, Paul Blaise, Olivier Henri-Rousseau. Best Performance of n^+ - p Crystalline Silicon Junction Solar Cells at 300 K, Due to the Effects of Heavy Doping and Impurity Size. I. *American Journal of Modern Physics.* Vol. 8, No. 2, 2019, pp. 18-36.
doi: 10.11648/j.ajmp.20190802.12

Received: June 5, 2019; **Accepted**: July 10, 2019; **Published**: July 24, 2019

Abstract: The effects of heavy doping and donor (acceptor) size on the hole (electron)-minority saturation current density $J_{Eo}(J_{Bo})$, injected respectively into the heavily (lightly) doped crystalline silicon (Si) emitter (base) region of n^+ - p junction, which can be applied to determine the performance of solar cells, being strongly affected by the dark saturation current density: $J_o \equiv J_{Eo} + J_{Bo}$, were investigated. For that, we used an effective Gaussian donor-density profile to determine J_{Eo}, and an empirical method of two points to investigate the ideality factor n, short circuit current density J_{sc}, fill factor (FF), and photovoltaic conversion efficiency η, expressed as functions of the open circuit voltage V_{oc}, giving rise to a satisfactory description of our obtained results, being compared also with other existing theoretical-and-experimental ones. So, in the completely transparent and heavily doped (P-Si) emitter region, CTHD(P-Si)ER, our obtained J_{Eo}-results were accurate within 1.78%. This accurate expression for J_{Eo} is thus imperative for continuing the performance improvement of solar cell systems. For example, in the physical conditions (PCs) of CTHD (P-Si) ER and of lightly doped (B-Si) base region, LD(B-Si)BR, we obtained the precisions of the order of 8.1% for J_{sc}, 7.1% for FF, and 5% for η, suggesting thus an accuracy of J_{Bo} ($\leq$ 8.1%). Further, in the PCs of completely opaque and heavily doped (S-Si) emitter region, COHD(S-Si)ER, and of lightly doped (acceptor-Si) base region, LD(acceptor-Si)BR, our limiting η-results are equal to: 27.77%,…, 31.55%, according to the E_{gi}-values equal to: 1.12eV ,…, 1.34eV, given in various (B,…, Tl)-Si base regions, respectively, being due to the acceptor-size effect. Furthermore, in the PCs of CTHD (donor-Si) ER and of LD(Tl-Si)BR, our maximal η-values are equal to: 24.28%,…, 31.51%, according to the E_{gi}-values equal to: 1.11eV ,…, 1.70eV, given in various (Sb,…, S)-Si emitter regions, respectively, being due to the donor-size effect. It should be noted that these obtained highest η-values are found to be almost equal, as: 31.51%%≃ 31.55%, coming from the fact that the two obtained limiting J_o-values are almost the same.

Keywords: Donor (Acceptor)-Size Effect, Heavily Doped Emitter Region, Ideality Factor, Open Circuit Voltage, Photovoltaic Conversion Efficiency

1. Introduction

The minority-carrier transport in the non-uniformly and heavily doped (NUHD), quasi-neutral, and uncompensated emitter region of impurity-silicon (Si) devices such as solar cells and bipolar transistors at temperature $T(= 300\ K)$, plays an important role in determining the behavior of many semiconductor devices [1-29]. It should be noted that the minority-carrier saturation current density, J_{Eo}, injected into this emitter region strongly controls the common emitter current gain [4-8]. Thus, an accurate determination of this J_{Eo} or an understanding of minority-carrier physics inside heavily doped semiconductors is imperative for continuing the performance improvement of bipolar transistors, and that of solar cell systems, which is commonly characterized in terms of the parameters such as: the ideality factor n, short circuit current density J_{sc}, fill factor FF, and photovoltaic conversion efficiency η, being

expressed as functions of the open circuit voltage V_{oc}[4]. Further, it should be noted that, in most fabricated silicon devices, the effective Gaussian donor-density profile $\rho(x)$, being proposed in next Equation (24), varies with carrier position x in the emitter region of width W [13, 18-20, 22], and it decreases with increasing W, being found to be in good agreement with that used by Essa et al. [13]. As a result, many other physical quantities, given in this NUHD n(p)-type thin emitter region such as [1-45]: the band gap narrowing (BGN), ΔE_g, Fermi energy E_F, apparent band gap narrowing (ABGN), ΔE_{ga}, minority-hole (electron) mobility $\mu_{h(e)}$, minority-hole (electron) lifetime $\tau_{h(e)}$, and minority-hole (electron) diffusion length $L_{h(e)}$, strongly depend on $\rho(x)$.

In the present paper, we determine an accurate expression for the minority-hole current density J_{Eo}, injected into the NUHD emitter region of $n^+ - p$ junction silicon solar cells at 300 K, being also applied to determine the performance of such crystalline silicon solar cells.

In Section 2, we study the effects of impurity size [or compression (dilatation)], temperature and heavy doping, affecting the energy-band-structure parameters such as: the intrinsic band gap E_{gi}, intrinsic carrier concentration n_i, band gap narrowing ΔE_g, Fermi energy E_F, apparent band gap narrowing ΔE_{ga}, and effective intrinsic carrier concentration n_{ie}. In Section 3, an accurate expression for the optical band gap (OBG), E_{g1}, is investigated in next Equation (16), being accurate within 1.86%, as showed in Table 3. Some useful minority-carrier transport parameters such as: μ_h and L_h, being given in the heavily doped n-type emitter region, and μ_e, τ_e and the minority-electron saturation current density J_{Bo}, being given in the lightly doped p-type base region, are also presented in Section 4. Then, in Section 5, an accurate expression for the minority-hole saturation current density J_{Eo}, injected into the heavily doped emitter region of $n^+ - p$ junction silicon solar cells at 300 K is established in Equation (39) or its approximate form given in Eq. (44), indicating an accuracy of the order of 1.78%, as seen in Table 4. Further, the total saturation current density: $J_o = J_{Eo} + J_{Bo}$, where J_{Bo} [1, 7], determined in Equation (21), is the minority-electron saturation current density J_{Bo}, injected into the lightly doped base region of $n^+ - p$ junction silicon solar cells, can be used to investigate the photovoltaic conversion effect, as presented in Section 6. Finally, some concluding remarks are given and discussed in Section 7.

2. Energy-Band-Structure Parameters in Donor (Acceptor)-Si Systems

Here, we study the effects of donor (acceptor) [d(a)]-size, temperature, and heavy doping on the energy-band-structure parameters of d(a)-Si systems, as follows.

2.1. Effect of d(a)-Size

In d(a)-Si-systems at T=0 K, since the d(a)-radius $r_{d(a)}$, in tetrahedral covalent bonds is usually either larger or smaller than the Si atom-radius r_o, assuming that in the P(B)-Si system $r_{P(B)} = r_o = 0.117$ nm, with $1\,\text{nm} = 10^{-9}\text{m}$, a local mechanical strain (or deformation potential energy) is induced, according to a compression (dilation) for $r_{d(a)} > r_o$ ($r_{d(a)} < r_o$), respectively, due to the d(a)-size effect. Then, in the Appendix A of our recent paper [42], basing on an effective Bohr model, such a compression (dilatation) occurring in various d(a)-Si systems was investigated, suggesting that the effective dielectric constant, $\varepsilon(r_{d(a)})$, decreases with increasing $r_{d(a)}$. This $r_{d(a)}$-effect thus affects the changes in all the energy-band-structure parameters, expressed in terms of $\varepsilon(r_{d(a)})$, noting that in the P(B)-Si system $\varepsilon(r_{P(B)}), = 11.4$. In particular, the changes in the unperturbed intrinsic band gap, $E_{go}(r_{P(B)}) = 1.17$ eV, and effective d(a)-ionization energy in absolute values $E_{do(ao)}(r_{P(B)}) = 33.58$ meV, are obtained in an effective Bohr model, as [42]:

$$E_{go}(r_{d(a)}) - E_{go}(r_{P(B)}) = E_{do(ao)}(r_{d(a)}) - E_{do(ao)}(r_{P(B)}) = E_{do(ao)}(r_{P(B)}) \times \left[\left(\frac{\varepsilon(r_{P(B)})}{\varepsilon(r_{d(a)})}\right)^2 - 1\right] \quad (1)$$

Therefore, with increasing $r_{d(a)}$, the effective dielectric constant $\varepsilon(r_{d(a)})$ decreases, implying that $E_{go}(r_{d(a)})$ increase. Those changes, which were investigated in our previous paper [42], are now reported in the following Table 1, in which the data of the critical d(a)-density $N_{cn(cp)}(r_{d(a)})$ are also reported. This critical density marks the metal-to-insulator transition from the localized side (all the impurities are electrical neutral), $N(N_a) \le N_{cn(cp)}(r_{d(a)})$, to the extended side, $N(N_a) \ge N_{cn(cp)}(r_{d(a)})$, assuming that all the impurities are ionized even at 0 K. However, at $T = 300$ K, for example, all the impurities are thus ionized and the physical conditions, defined by: $N(N_a) > N_{cn(cp)}(r_{d(a)})$ and $N(N_a) < N_{cn(cp)}(r_{d(a)})$, can thus be used to define the n(p)-type heavily and lightly doped Si, respectively.

Table 1. *The values of $r_{d(a)}$, $\varepsilon(r_{d(a)})$, and $E_{go}(r_{d(a)})$, and critical impurity density $N_{cn(cp)}(r_{d(a)})$, obtained in our previous paper [42], are reported here.*

Donor	**Sb**	**P**	**As**	**Bi**	**Ti**	**Te**	**Se**	**S**
T=0 K								
r_d (nm)	0.1131	0.1170	0.1277	0.1292	0.1424	0.1546	0.1621	0.1628
$\varepsilon(r_d)$	12.02	11.40	8.47	7.95	4.71	3.26	2.71	2.67
$E_{go}(r_d)$(eV)	1.167	1.170	1.197	1.205	1.333	1.547	1.729	1.749
$N_{cn}(r_d)(10^{18}\ \text{cm}^{-3})$	3	3.52	8.58	10.37	50	150.74	261.24	274.57

Acceptor	B	Al	Ga	In	Tl
T=0 K					
r_a (nm)	0.1170	0.1254	0.1263	0.1352	0.1410
$\varepsilon(r_a)$	11.40	8.88	8.49	5.57	4.42
$E_{go}(r_d)$ (eV)	1.170	1.195	1.201	1.292	1.387
$N_{cp}(r_a)(10^{18}\ cm^{-3})$	4.06	8.58	9.83	34.73	69.87

2.2. Temperature Effect

Being inspired from excellent works by Pässler [33, 34], who used semi-empirical descriptions of T-dependences of band gap of the Si by taking into account the cumulative effect of electron-phonon interaction and thermal lattice expansion mechanisms or all the contributions of individual lattice oscillations [33-35], we proposed in our recent paper [43] a simple accurate expression for the intrinsic band gap in the silicon (Si), due to the T-dependent carrier-lattice interaction-effect, $E_{gi}(T, r_{d(a)})$, by

$$E_{gi}(T, r_{d(a)}) \simeq E_{go}(r_{d(a)}) - 0.071\ (eV) \times \left\{\left[1 + \left(\frac{2T}{440.6913\ K}\right)^{2.201}\right]^{\frac{1}{2.201}} - 1\right\} \quad (2)$$

where the values of $E_{go}(r_{d(a)})$ due to the d(a)-size effect are given in Table 1 and those of $E_{gi}(T = 300\ K, r_{d(a)})$ tabulated in Table 2. Further, as noted in this Reference 43, in the (P, S)-Si systems, for $0\ K \le T \le 3500\ K$, the absolute maximal relative errors of this E_{gi}-result were found to be equal respectively to: 0.22% and 0.15%, calculated using the very accurate complicated results given by Pässler [34]. Then, in the n-type HD silicon at temperature T, the effective mass of the majority electron can be defined by [31, 32]:

$$m_c(T, r_d) = \left[0.9163 \times \left(0.1905 \times \frac{E_{go}(r_d)}{E_{gi}(T, r_d)}\right)^2\right]^{1/3} \times m_o = m_{eo} \times \left(\frac{E_{go}(r_d)}{E_{gi}(T, r_d)}\right)^{2/3} \quad (3)$$

which gives: $m_{eo} = m_e(T = 0\ K) = 0.3216 \times m_o$, m_o being the electron rest mass, and the effective mass of the minority hole yields [31, 32]:

$$m_v(T) = g_v^{-2/3} \times \left(\frac{0.443587 + 0.3609528\times10^{-2}T + 0.1173515\times10^{-3}T^2 + 0.1263218\times10^{-5}T^3 + 0.3025581\times10^{-8}T^4}{1 + 0.4683382\times10^{-2}T + 0.2286895\times10^{-3}T^2 + 0.7469271\times10^{-6}T^3 + 0.1727481\times10^{-8}T^4}\right)^{2/3} \quad (4)$$

which gives $m_v(T = 0\ K) = m_{vo} = 0.3664 \times m_o$. Here, $g_v = 2$ is the effective average number of equivalent valence-band edges. Now, the intrinsic carrier concentration n_i is defined by

$$n_i^2(T, r_{d(a)}, g_c) \equiv N_c(T, r_d, g_c) \times N_v(T, g_v) \times \exp\left(\frac{-E_{gi}(T, r_{d(a)})}{k_B T}\right) \quad (5)$$

where, $N_{c(v)}$ is the conduction (valence)-band density of states, given by [31, 32]:

$$N_c(T, r_d, g_c) = 2g_c \times \left(\frac{m_c(T, r_d) \times k_B T}{2\pi\hbar^2}\right)^{\frac{3}{2}} (cm^{-3}) \quad (6)$$

$$N_v(T, g_v) = 2g_v \times \left(\frac{m_v(T) \times k_B T}{2\pi\hbar^2}\right)^{\frac{3}{2}} (cm^{-3}) \quad (7)$$

where $\hbar = h/2\pi$ is the Dirac's constant, k_B is the Boltzmann constant, and g_c is the effective average number of equivalent conduction-band edges. Moreover, for $r_d \equiv r_P$ and at 300 K, some typical n_i-results obtained for different g_c-values, calculated using Equation (5), are given as follows.

(i) If $g_c = 6$, one then gets: $n_i = 10.7 \times 10^9\ cm^{-3}$, being just a result investigated from a measurement of energy-band-structure parameters and intrinsic conductivity by Green [31].

(ii) If $g_c = 5$, one then obtains: $n_i = 9.77 \times 10^9\ cm^{-3}$, according to a result given from a capacitance measurement of a pin diode biased under high injection, by Misiakos and Tsamakis [37].

(iii) Finally, if $g_c = 4.9113$, one then gets: $n_i = 9.68 \times 10^9\ cm^{-3}$, according to a result proposed by Couderc et al. (C) as [38]: $n_{i(C)} = 1.541 \times 10^{15} \times T^{1.721} \times \exp\left(-\frac{E_{gi}}{2kT}\right)\ cm^{-3} = 9.68 \times 10^9\ cm^{-3}$ for T=300 K, basing on their updated fit of experimental data for the minority-carrier mobility and open-circuit voltage decay, which were given by Sproul and Green [36].

Further, from Equations (5, 2), in donor-Si systems and for T=300 K, the numerical results of n_i and E_{gi}, calculated for $g_c = 6, 5, and\ 4.9113$, as functions of $r_{d(a)}$, are tabulated in Table 2.

Table 2. *The values of intrinsic carrier concentration $n_i(T = 300\ K, r_{d(a)}, g_c)$ and intrinsic band gap E_{gi} are calculated for $g_c = 6, 5, and\ 4.9113$, using Equations (5, 2), respectively, as functions of $r_{d(a)}$.*

Donor	Sb	P	As	Bi	Ti	Te	Se	S
$g_c = 6$								
E_{gi}(300K) in eV	1.1215	1.1245	1.1515	1.1595	1.2875	1.5015	1.6835	1.7035
n_i(300K) in $10^{10}\ cm^{-3}$	1.13	1.07	6.34×10^{-1}	5.43×10^{-1}	4.56×10^{-2}	7.26×10^{-4}	2.14×10^{-5}	1.46×10^{-5}

Donor	**Sb**	**P**	**As**	**Bi**	**Ti**	**Te**	**Se**	**S**
$g_c = 5$								
$n_i(300K)$ in 10^{10} cm^{-3}	1.04	9.77×10^{-1}	5.79×10^{-1}	4.96×10^{-1}	4.17×10^{-2}	6.63×10^{-4}	1.96×10^{-5}	1.33×10^{-5}
$g_c = 4.9113$								
$n_i(300K)$ in 10^{10} cm^{-3}	1.03	9.68×10^{-1}	5.74×10^{-1}	4.92×10^{-1}	4.13×10^{-2}	6.57×10^{-4}	1.94×10^{-5}	1.32×10^{-5}

Acceptor	**B**	**Al**	**Ga**	**In**	**Tl**
$g_c = 6$					
$E_{gi}(300K)$ in eV	1.1245	1.1495	1.1555	1.2465	1.3415
$n_i(300\ K)$ in 10^{10} cm^{-3}	1.07	6.59×10^{-1}	5.87×10^{-1}	1.01×10^{-1}	1.60×10^{-2}

From those results, one remarks that, for T=300 K, n_i decreases with increasing $r_{d(a)}$ since $E_{gi}(T, r_{d(a)})$ increases, being due to the d(a)-size effect.

2.3. Heavy Doping Effect

First of all, in the donor-Si system, we define the effective intrinsic carrier concentration n_{ie}, by

$$n_{ie}^2 \equiv N \times p_o \equiv n_i^2 \times \exp\left[\frac{\Delta E_{ga}}{k_B T}\right] \quad (8)$$

where n_i^2 is determined in Equation (5). Here, we can also define the "effective doping density" by [8]: $N_{Deff.} \equiv N/\exp\left[\frac{\Delta E_{ga}}{k_B T}\right]$ so that $N_{Deff.} \times p_o \equiv n_i^2$. Here, p_o is the density of minority holes at the thermal equilibrium and the ABGN is defined by:

$$\Delta E_{ga} \equiv \Delta E_g + k_B T \times \ln\left(\frac{N}{N_C}\right) - E_F \quad (9)$$

where N_C is defined in Equation (6), the Fermi energy E_F due to the effects of heavy doping and Fermi-Dirac statistics is determined in Equation (A3) of the Appendix A, being accurate within 2.11×10^{-4} [39], and the BGN, ΔE_g, due to the heavy doping effect, is determined in Equation (A9) of the Appendix B.

Furthermore, in order to determine the minority-carrier saturation current J_{Eo}, injected into the uniformly and heavily doped emitter region of the silicon devices, Jain and Roulston (JR) [15], Klaassen, Slotboom and Graaff (KSG) [16], Zouari and Arab (ZA) [17], Stem and Cid (SC) [18], and Yan and Cuevas (YC) [19], proposed their empirical expressions for the ABGN, being obtained in the P-Si system at 300 K, by:

$$\Delta E_{ga(JR)}(N) = 8.5\times10^{-3} \times \left\{\ln\left(\frac{N}{3.5\times10^{17}\ cm^{-3}}\right) + \sqrt{\left[\ln\left(\frac{N}{3.5\times10^{17}\ cm^{-3}}\right)\right]^2 + 0.5}\right\}\ (eV) \quad (10)$$

$$\Delta E_{ga(KSG)}(N) = 6.92\times10^{-3} \times \left\{\ln\left(\frac{N}{1.3\times10^{17}\ cm^{-3}}\right) + \sqrt{\left[\ln\left(\frac{N}{1.3\times10^{17}\ cm^{-3}}\right)\right]^2 + 0.5}\right\}\ (eV) \quad (11)$$

$$\Delta E_{ga(ZA)}(N) = 18.7\times10^{-3} \times \ln\left(\frac{N}{7\times10^{17}\ cm^{-3}}\right)\ (eV) \quad (12)$$

$$\Delta E_{ga(SC)}(N) = 14\times10^{-3} \times \ln\left(\frac{N}{1.4\times10^{17}\ cm^{-3}}\right)\ (eV) \quad (13)$$

$$\Delta E_{ga(YC)}(N) = 4.2\times10^{-5} \times \left[\ln\left(\frac{N}{10^{14}\ cm^{-3}}\right)\right]^3\ (eV) \quad (14)$$

Then, in such the P-Si system at 300K, being inspired by the term: $k_B T \times \ln\left(\frac{N}{N_C}\right)$ given in Equation (9), and also by the result: $\Delta E_{ga(YC)}(N)$ given in Equation (14), we can now propose a modified (Mod.) YC-model for the ABGN so that its numerical results are found to be closed to those calculated by using Equation (9), as:

$$\Delta E_{ga(Mod.YC)}(N, g_c) = 114.94\times10^{-6} \times \left[\ln\left(\frac{5.7167\times10^3}{N_C} \times \frac{N\times6}{g_c}\right)\right]^3\ (eV) = 114.94\times10^{-6} \times \left[\ln\left(\frac{N\times\left(\frac{6}{g_c}\right)}{5\times10^{15}\ cm^{-3}}\right)\right]^3\ (eV) \quad (15)$$

having a same empirical form as that given in Equation (14).

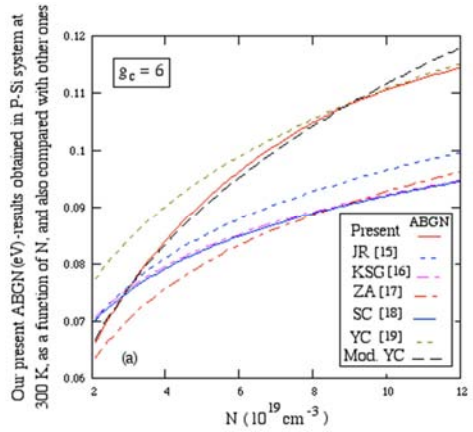

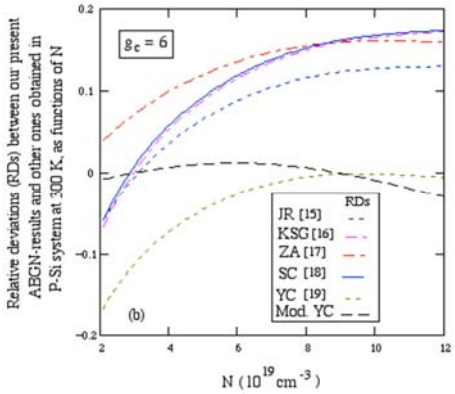

Figure 1. *(a, b) our ABGN-results given in heavily doped donor-Si systems, with a condition: $N > N_{cn}(r_d)$.*

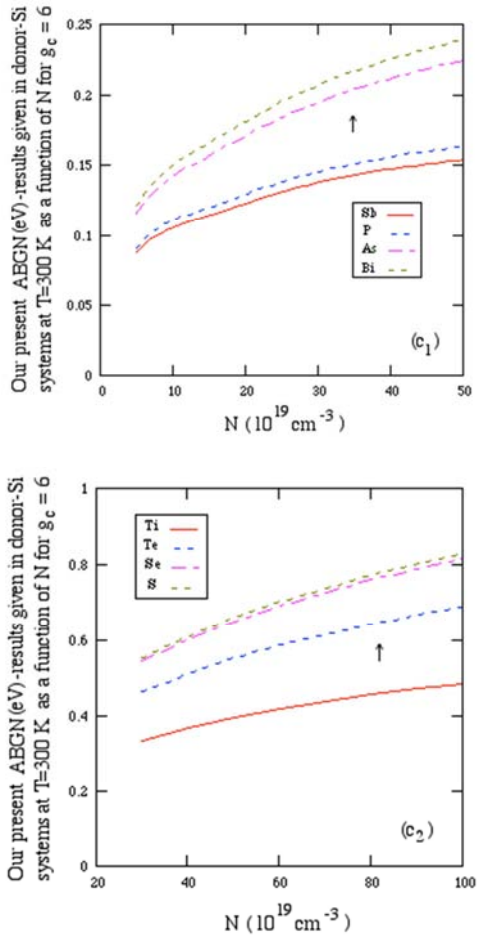

Figure 2. *(c_1, c_2) our ABGN-results given in heavily doped donor-Si systems, with a condition: $N > N_{cn}(r_d)$.*

Now, for $g_c = 6$, in d-Si systems at 300 K, our numerical ABGN (ΔE_{ga})-results are calculated, using Equation (9). First, ours, obtained for the P-Si system, are plotted as a function of N in Figure 1 (a), in which, for a comparison, the other ones, calculated using Equations (10-15), are also included. Secondly, in this P-Si system, the relative deviations between ours and the others are also plotted as functions of N in Figure 1 (b). Finally, in Figure 2 (c_1, c_2), ours are plotted in donor-Si systems as functions of N.

Here, one observes that:

(i) our numerical ABGN-results obtained using Equations (9, 15) are found to be closed together as seen in Figure 1 (a), and their absolute maximal relative deviation yields: 3.03%, which occurs at $N = 1.2 \times 10^{20}$ cm^{-3}, as observed in Figure 1 (b), and

(ii) in Figure 2 (c_1, c_2), for a given donor-Si system, due to the heavy doping effect, ours increase with increasing N, and for a given N, ours increase (↑) with increasing r_d, due to the donor-size effect.

Then, in the following, it is possible to define the optical band gap (OBG), expressed in terms of the ABGN (or BGN), suggesting a conjunction between the electrical-and-optical phenomena.

3. Conjunction Between Electrical-and-Optical Phenomena

First of all, we define the optical band gap (OBG) by [25]:

$$E_{g1}(N, T, r_d, g_c) \equiv E_{gi}(T, r_d) - \Delta E_g\,(N, T, r_d, g_c) + E_F(N, T, r_d, g_c) \tag{16}$$

where the intrinsic band gap E_{gi} is determined in Equation (2), the BGN ΔE_g is investigated in Equation (A9) of the Appendix B, and the Fermi energy E_F is given in Equation (A3) of the Appendix A, suggesting that the optical phenomenon is represented by E_{g1}. Furthermore, it is possible to establish a conjunction between the electrical and optical phenomena, obtained from Equations (9, 16), as:

$$E_{g1}(N, T, r_d, g_c) \equiv E_{gi}(T, r_d) - \Delta E_{ga}\,(N, T, r_d, g_c) + k_B T \times \ln\left(\frac{N}{N_C(T, r_d, g_c)}\right)$$

which can be rewritten, for example, replacing ΔE_{ga} by $\Delta E_{ga(Mod.YC)}(N)$ determined in Equation (15), as:

$$E_{g1(Mod.YC)}(N, T, r_d, g_c) \equiv E_{gi}(T, r_d) - \Delta E_{ga(Mod.YC)}(N, g_c) + k_B T \times \ln\left(\frac{N}{N_C(T, r_d, g_c)}\right) \tag{17}$$

Now, in the P-Si system, our numerical OBG-results, calculated using Equations (16, 17) for $g_c = 6, 5, 4.9113$ and at T=300 K, are tabulated in following Table 3, in which our numerical results of E_{g1} and $E_{g1(Mod.YC)}$, obtained for $g_c = 6$, are accurate within 1.86% and 1.9%, respectively, and found to be the best ones, compared with those obtained for $g_c = 5, 4.9113$. One notes that the relative deviations (RDs) between calculated E_{g1}-results and E_{g1}-data [44] are defined by: $1 - \frac{\text{Calculated } E_{g1}\text{-results}}{E_{g1}\text{-data}}$.

Table 3. *Our numerical results of optical band gap (OBG), expressed as functions of N for $g_c = 6, 5, 4.9113$, and their relative deviations.*

N (10^{18} cm^{-3})	**4**	**8.5**	**15**	**50**	**80**	**150**
E_{g1}(eV)-data [44]	1.020	1.028	1.033	1.050	1.056	1.059
Our OBG-results are obtained, using Equation (16).						
$g_c = 6$						
E_{g1}(eV)	1.0390	1.0465	1.0496	1.0483	1.0463	1.0479
RD(%)	-1.86	-1.80	-1.61	0.17	0.92	1.05

N (10^{18} cm^{-3})	**4**	**8.5**	**15**	**50**	**80**	**150**
$g_c = 5$						
E_{g1}(eV)	1.0411	1.0478	1.0501	1.0473	1.0462	1.0470
RD(%)	-2.07	-1.92	-1.66	0.25	0.92	1.14
$g_c = 4.9113$						
E_{g1}(eV)	1.0413	1.0479	1.0502	1.0473	1.0463	1.0468
RD(%)	-2.09	-1.93	-1.66	0.26	0.92	1.15
Other OBG-results are obtained from Equation (17).						
$g_c = 6$						
$E_{g1(Mod.YC)}$(eV)	1.0394	1.0459	1.0489	1.0492	1.0469	1.0415
RD(%)	-1.90	-1.74	-1.54	0.08	0.86	1.66
$g_c = 5$						
$E_{g1(Mod.YC)}$(eV)	1.0412	1.0470	1.0495	1.0485	1.0456	1.0394
RD(%)	-2.08	-1.85	-1.59	015	0.98	1.85
$g_c = 4.9113$						
$E_{g1(Mod.YC)}$(eV)	1.0414	1.0471	1.0495	1.0484	1.0454	1.0392
RD(%)	-2.09	-1.86	-1.60	0.15	0.99	1.87

The underlined $|RD|$-values are the maximal ones.

Here, our best choice is $g_c = 6$, meaning that at $T \geq 300$ K, due to the high thermal agitation energy k_BT, all the six equivalent conduction-band edges are effective.

4. Minority-Carrier Transport Parameters

Here, in the heavily doped n-type emitter region and the lightly doped p-type base region of $n^+ - p$ junction silicon solar cells, the minority-hole (electron) transport parameters are studied as follows.

4.1. Heavily Doped n-type Emitter-region Parameters

In order to determine the minority-hole saturation-current density J_{Eo}, injected into the heavily doped n-type emitter-region, we need to know an expression for the minority-hole mobility μ_h, being related to the minority-hole diffusion coefficient D_h, by the well-known Einstein relation: $D_h = \frac{k_BT}{e} \times \mu_h$, where e is the positive hole charge. Here, in donor-Si systems at 300 K and for any g_c, since the minority-hole mobility depends on N [10], and also on g_c and $\varepsilon(r_d)$ [11], we can propose:

$$\mu_h(N, T, r_d, g_c) = \left[130 + \frac{500-130}{1+\left(\frac{N\times 6}{8\times 10^{17}\,cm^{-3}\times g_c}\right)^{1.25}}\right] \times \left(\frac{\varepsilon(r_d)}{\varepsilon(r_P)}\right)^2 \times \left(\frac{T}{300\,K}\right)^{3/2} (cm^2V^{-1}s^{-1}) \quad (18)$$

noting that as T = 300 K, $g_c = 6$, and $r_d \equiv r_P$, Equation (18) is reduced to that given by del Alamo et al. [10]. Moreover, Equation (18) indicates that, for a given N and with increasing r_d, μ_h decreases, since $\varepsilon(r_d)$ decreases as seen in Table 1, being due to the d-size effect, in good accordance with that observed by Logan et al. [9]. Further, from Equations (5, 8, 9, 15, 18), we can define the following minority-hole transport parameter F as [22, 25]:

$$F(N, T, r_d, g_c) \equiv \frac{n_i^2}{p_o \times D_h} = \frac{N_{Deff.}}{D_h} \equiv \frac{N}{D_h \times \exp\left[\frac{ABGN}{k_BT}\right]}\ (cm^{-5} \times s), \quad (19)$$

where $N_{Deff.}$ is the "effective doping density" [8] and the ABGN is determined in Equation (9) for our ΔE_{ga}-result or in Equation (15) for our approximate $\Delta E_{ga(Mod.YC)}$-one.

Furthermore, the minority-hole length, $L_h(N, T, r_d, g_c) = \sqrt{\tau_h \times D_h}$, τ_h being the minority-hole lifetime, can be determined by [22, 25]:

$$L_h^{-2}(N, T, r_d, g_c) = [\tau_h \times D_h]^{-1} = (C \times F)^2 = \left(C \times \frac{N_{Deff.}}{D_h}\right)^2 = \left(C \times \frac{n_i^2}{p_o \times D_h}\right)^2 \quad (20)$$

where the constant $C[= 10^{-17}\ (cm^4/s)]$ was chosen in this work. Here, one remarks that τ_h can be computed since D_h (or μ_h) and F are determined respectively in Equations (18, 19).

4.2. Lightly Doped p-type Base-Region Parameters

Here, the minority-electron saturation current density injected into the lightly doped p-type base region, with an acceptor density equal to N_a, is given by [1, 7]:

$$J_{Bo}(N_a, T, r_a) = \frac{e \times n_i^2(T, r_a, g_c=6) \times \sqrt{\frac{D_e(N_a, T, r_a)}{\tau_e(N_a)}}}{N_a} \quad (21)$$

where $n_i^2(T, r_{d(a)}, g_c = 6)$ is determined in Equation (5) and $D_e(N_a, T, r_a) \equiv \frac{k_BT}{e} \times \mu_e(N_a, T, r_a)$ is the minority-electron diffusion coefficient, noting that Equation (21) is valid only for $N_a \leq 10^{16}$ cm^{-3}.

Here, in the acceptor-Si system, μ_e is the minority-electron mobility, being determined by [3, 11, 16]:

$$\mu_e(N_a, T, r_a) = \left[92 + \frac{1360-92}{1+\left(\frac{N_a}{1.3\times 10^{17}\,cm^{-3}}\right)^{0.91}}\right] \times \left(\frac{\varepsilon(r_a)}{\varepsilon(r_B)}\right)^2 \times \left(\frac{T}{300\,K}\right)^{3/2} (cm^2V^{-1}s^{-1}) \quad (22)$$

being reduced to the result obtained by Slotbottom and de Graaff [3, 16], as T=300 K and $r_a = r_B$, and $\tau_e(N_a)$ is the

minority-electron lifetime, computed by [16, 25]:

$$\tau_e(N_a)^{-1} = \frac{1}{2.5\times10^{-3}} + 3\times10^{-13}\times N_a + 1.83\times10^{-31}\times N_a^2. \quad (23)$$

Furthermore, Equation (22) indicates that, for a given N_a and with increasing r_a, μ_h decreases, since $\varepsilon(r_a)$ decreases, as seen in Table 1, in good accordance with that observed by Logan et al. [9].

Then, in P(B)-Si systems at 300 K and for $g_c = 6$, Klaassen et al. confirmed, in Figures 1 and 2 of their paper [16], that the expressions (18, 22) for minority-hole (electron) mobility $\mu_{h(e)}$ are simple and accurate.

In the following, we will determine the minority-hole saturation-current density J_{Eo}, injected into the heavily doped n-type emitter-region of the $n^+ - p$ junction solar cells.

5. Minority-Hole Saturation Current Density

Let us first propose in the non-uniformly and heavily doped (NUHD) emitter region of donor-Si devices our expression for the effective Gaussian donor-density profile or the donor (majority-electron) density, defined in the emitter-region width W, by:

$$\rho(x) = N\times\exp\left\{-\left(\frac{x}{W}\right)^2\times\ln\left[\frac{N}{N_o(W)}\right]\right\} \equiv N\times\left[\frac{N}{N_o(W)}\right]^{-\left(\frac{x}{W}\right)^2} \quad (24)$$

where $N_o(W) \equiv 7.9\times10^{17}\times\exp\left\{-\left(\frac{W}{0.1842\ \mu m}\right)^{1.066}\right\}$ (cm^{-3}), $1\ \mu m = 10^{-4}$ cm, decreases with increasing W, in good agreement with the doping profile measurement on silicon devices, studied by Essa et al. [13]. Moreover, Equation (24) indicates that:

(i) at the surface emitter: x=0, $\rho(0) = N$, defining the surface donor density, and

(ii) at the emitter-base junction: x=W, $\rho(W) = N_o(W)$, which decreases with increasing W, as noted above. Here, we also remark that $N_{o(VCD)} = 7\times10^{17}\ cm^{-3}$ was proposed by Van Cong and Debiais (VCD) [22], and $N_{o(ZA)} = 2\times10^{16}\ cm^{-3}$, by Zouari and Arab (ZA) [17], for their Gaussian impurity density profile. Moreover, all the parameters given in Equation (24) were chosen such that the errors of our obtained J_{Eo}–values are minimized, as seen in next Table 4, and our numerical calculation indicates that, from Equation (24), we can determine the highest value of W, being equal here to 85 μm.

Now, from Equations (8, 9) or Equation (19), taken for $0 \le x \le W$, and using Equation (24), the result: $N_{Deff.}(x = 0) \equiv N/\exp\left[\frac{\Delta E_{ga}(N)}{k_BT}\right]$ may be rewritten as:

$$N_{Deff.}(x) \equiv \rho(x)/\exp\left[\frac{\Delta E_{ga}(\rho(x))}{k_BT}\right] \quad (25)$$

which gives at x=W: $N_{Deff.}(W) \equiv \frac{N_o(W)}{\exp\left[\frac{\Delta E_{ga}(N_o(W))}{k_BT}\right]}$.

Then, under low-level injection, in the absence of external generation, and for the steady-state case, we can define the minority-hole density by:

$$p_o(x) \equiv \frac{n_i^2}{N_{Deff.}(x)} \quad (26)$$

and a normalized excess minority-hole density [or a relative deviation between $p(x)$ and $p_o(x)$] by [22, 25]:

$$u(x) \equiv \frac{p(x)-p_o(x)}{p_o(x)} \quad (27)$$

which must verify the two following boundary conditions proposed by Shockley as [2]:

$$u(x=0) \equiv \frac{-J_h(x=0)}{eS\times p_o(x=0)} \quad (28)$$

$$u(x=W) \simeq \exp\left(\frac{V}{n(V)\times V_T}\right) - 1, \text{for small W} - \text{values} \quad (29)$$

Here, $n(V)$ is an ideality factor, S $(\frac{cm}{s})$ is the hole surface recombination velocity at the emitter contact, V is the applied voltage, $V_T \equiv (k_BT/e)$ is the thermal voltage, and the minority-hole current density $J_h(x)$, being found to be similar to the Fick's law for diffusion equation, is given by [8, 22]:

$$J_h(x) = -\frac{en_i^2}{F(x)}\times\frac{du(x)}{dx} = -\frac{en_i^2 D_h(x)}{N_{Deff.}(x)}\times\frac{du(x)}{dx} \quad (30)$$

where $F(x)$ is determined in Equation (19), in which N is replaced by $\rho(x)$, proposed in Equation (24).

Further, the minority-hole continuity equation yields [8, 22]:

$$\frac{dJ_h(x)}{dx} = -en_i^2\times\frac{u(x)}{F(x)\times L_h^2} = -en_i^2\times\frac{u(x)}{N_{Deff.}(x)\times\tau_h(\rho(x))} = -e\times[p(x)-p_0(x)]\times\frac{\tau_h(N)}{\tau_h(\rho(x))}\times\frac{1}{\tau_h(N)}. \quad (31)$$

Then, from these two Equations (30, 31), one obtains the following second-order differential equation as [22]:

$$\frac{d^2u(x)}{dx^2} - \frac{dF(x)}{dx}\times\frac{du(x)}{dx} - \frac{u(x)}{L_h^2(x)} = 0 \quad (32)$$

Using the two boundary conditions (28, 29), one thus gets the general solution of this Equation (32) as [22]:

$$u(x) = \left[A(W)\times\sinh(P(x)) + B(W)\times\cosh(P(x))\right]\times\left(\exp\left(\frac{V}{n(V)\times V_T}\right) - 1\right) \quad (33)$$

where $A(W) \equiv \frac{1}{\sinh(P(W))+I(W)\times\cosh(P(W))}$, $I(W,S) \equiv \frac{B}{A} = \frac{D_h(N_o(W))}{S\times L_h(N_o(W))}$ and $P(x) \equiv \int_0^x C\times F(x)dx$, since $\frac{dP(x)}{dx} \equiv C\times F(x)$. Here, $C = 10^{-17}\ (cm^4/s)$, as that chosen in Equation (20), and the hyperbolic sine-and-cosine functions are defined by: $\sinh(x) \equiv 0.5\times[e^x - e^{-x}]$ and $\cosh(x) \equiv 0.5\times[e^x + e^{-x}]$.

Further, from Eq. (33), as $P(W) \ll 1$ (or for small W) one has: $A \simeq \frac{1}{I}$ or $B \simeq 1$, and one therefore obtains: $u(W) \simeq \left[\exp\left(\frac{V}{n(V)\times V_T}\right) - 1\right]$, which is just the boundary condition given in Equation (29). Now, using Equations (30, 33), one gets:

$$J_h(x, N, T, r_d, g_c, S) = -J_{Eo}(x, N, T, r_d, g_c, S) \times \left(\exp\left(\frac{V}{n(V)\times V_T}\right) - 1\right) \quad (34)$$

where J_{Eo} is the minority-hole saturation current density, being injected into the heavily doped n-type emitter region for $0 \le x \le W$ and given by:

$$J_{Eo}(x, N, T, r_d, g_c, S) = en_i^2 C \times \left[A(W) \times \cosh(P(x)) + B(W) \times \sinh(P(x))\right] \quad (35)$$

One also remarks that, from Equations (20, 33-35) and after some manipulations, one gets: $u(x = 0) \equiv \frac{-J_h(x=0)}{eS \times p_o(x=0)}$, being just the boundary condition given in Eq. (28). Now, using the P(x)-definition given in Equation (33), at T=300 K, one can define the inverse effective minority-hole diffusion length by:

$$\frac{1}{L_{h,eff.}(x=W,N,T,r_d,g_c)} = \frac{1}{W}\int_0^W \frac{dx}{L_h(x)} = \frac{1}{W}\int_0^W C \times F(x)dx \equiv P(x = W, N, T, r_d, g_c)/W \quad (36)$$

where $L_h = (CF)^{-1}$ is defined in Equation (20), in which N is replaced by $\rho(x)$, being determined in Equation (24). Therefore, Equation (36) can be rewritten as:

$$P(x = W, N, r_d, g_c) \equiv \frac{W}{L_{h,eff.}} = \frac{W}{L_h} \times \frac{L_h}{L_{h,eff.}} \quad (37)$$

for a simplicity. Then, from Eq. (33, 35), since $B = A \times I(W, S)$ one obtains:

$$J_{Eo}(x = 0, N, r_d, g_c, S) = en_i^2 C \times A = \frac{en_i^2 C}{\sinh(P)+I\times\cosh(P)} \quad (38)$$

$$J_{Eo}(x = W, N, r_d, g_c, S) = en_i^2 C \times \frac{\cosh(P)+I\times\sinh(P)}{\sinh(P)+I\times\cosh(P)} \quad (39)$$

Now, from those results (34, 38, 39), one gets:

$$\frac{J_h(x=0,N,r_d,g_c,S)}{J_h(x=W,N,r_d,g_c,S)} \equiv \frac{J_{Eo}(x=0,N,r_d,g_c,S)}{J_{Eo}(x=W,N,r_d,g_c,S)} = \frac{1}{\cosh(P)+I\times\sinh(P)} \quad (40)$$

Further, using Equations (27, 33, 34) and going back to the minority-hole continuity equation defined in Equation (31), one gets:

$$\frac{1}{J_{Eo}(x=W)} \times \left[J_{Eo}(x = W) - J_{Eo}(x = 0) = \frac{1}{\tau_h(N)} \times Q_{h,eff.}(x = W, N)\right], \quad (41)$$

where $\tau_h(N, r_d, g_c)$ is determined in Equation (20), and $Q_{h,eff.}(C/cm^2)$ is the effective excess minority-hole charge density given in the emitter region, defined by [22]:

$$Q_{h,eff.}(x = W, N) \equiv \int_0^W e \times [p(x) - p_0(x)] \times \frac{\tau_h(N)}{\tau_h(\rho(x))}dx. \quad (42)$$

Finally, from Equations (40, 41), if defining the effective minority-hole transit time by: $\tau_{t,eff.}(x = W, N, S) \equiv Q_{h,eff.}(x = W, N)/J_{Eo}(x = W, N, r_d, g_c, S)$, one then obtains the reduced effective minority-hole transit time, as:[22]

$$\frac{\tau_{t,eff.}(x=W,N,r_d,g_c,S)}{\tau_h} = 1 - \frac{J_{Eo}(x=0,N,r_d,g_c,S)}{J_{Eo}(x=W,N,r_d,g_c,S)} = 1 - \frac{1}{\cosh(P)+I\times\sinh(P)}. \quad (43)$$

Now, from above Equations (38-43), some important results can be obtained and discussed below.

5.1. Very Large $S(= 10^{50}\ \frac{cm}{s}$, For Example) or $S \to \infty$ and $P \ll 1$ or $W \ll L_{h,eff}$.

Here, various results can be investigated as follows.

(i) From Equations (38-40), since $I(W) = \frac{D_h(N_o(W))}{S\times L_h(N_o(W))} \to 0$ as $S \to \infty$, $\frac{J_{Eo}(x=0,N,r_d,g_c,S)}{J_{Eo}(x=W,N,r_d,g_c,S)} \simeq \frac{1}{\cosh(P)} \to 1$ since $P \ll 1$, or $J_{Eo}(x = W, N, r_d, g_c, S \to \infty) \simeq J_{Eo}(x = 0, N, r_d, g_c, S \to \infty)$. Therefore, from Equation (43), one obtains: $\frac{\tau_{t,eff.}(x=W,N,r_d,g_c,S\to\infty)}{\tau_h(N)} \to 0$, suggesting a completely transparent emitter region (CTER).

(ii) Further, from Equations (18-20, 39), since $I \to 0$ and $P \ll 1$, the result (39) is now reduced to:

$$J_{Eo}(x = W, N, r_d, g_c, S \to \infty) \simeq \frac{en_i^2 C}{P} = \frac{en_i^2}{F\times W} \times \frac{L_{h,eff.}}{L_h} = \frac{en_i^2 \times D_h}{N_{Deff}\times W} \times \frac{L_{h,eff.}}{L_h} \quad (44)$$

being found to be independent of S and C, since $\frac{L_{h,eff.}}{L_h}$ is independent of S and C as observed in Equations (20, 36), and noting that the ABGN-expression is determined by Equation (9) or by Equation (15).

Now, in the P-Si system, for $T = 300$ K, $r_d \equiv r_P$ and $g_c = 6, 5, 4.9113$, our two numerical J_{Eo}-results are calculated, using Equations (44, 9) and (44, 15), and given in Table 4, in which the CTER -condition, $P \ll 1$ (or $\frac{\tau_{t,eff.}}{\tau_h(N)} \ll 1$), is fulfilled, and we also compare them with modeling and measuring J_{Eo}-results investigated by del Alamo et al. (ASS) [10, 12]. One notes that their modeling J_{Eo}-result [10], based only on two independent parameters: N_{Deff}/D_h and L_h, can be obtained, for $L_{h,eff.} = W$, from our above result (44). This could explain a great difference between their modeling results [10, 12], being accurate within 36%, and ours, accurate within 1.78%, for $g_c = 6$, as those observed in the following Table 4.

Table 4. *Our present results of J_{Eo} ($\frac{A}{cm^2}$) expressed as functions of N for $g_c = 6, 5, 4.9113$, and their relative deviations (RDs), calculated by: RD(%)=1-(Present J_{Eo}/ J_{Eo}-data), where the J_{Eo} ($\frac{A}{cm^2}$)-data are given in References 10 and 12, the theoretical ASS-J_{Eo} ($\frac{A}{cm^2}$)-results, obtained by Alamo et al. (ASS) [10, 12], and also their relative deviations.*

N (10^{19} cm^{-3})	**2.1**	**3.3**	**4.4**	**4.6**	**12**
W (μm)	0.20	1.00	0.23	0.66	0.20
$J_{Eo}(S \to \infty)$−data	3.2×10^{-12}	8.3×10^{-13}	2.6×10^{-12}	1.1×10^{-12}	2.8×10^{-12}
ASS- $J_{Eo}(S \to \infty)$]	3.6×10^{-12}	1.1×10^{-12}	2.6×10^{-12}	1.5×10^{-12}	2.81×10^{-12}
RD(%)	-12.5	-32.5	0	-36	-0.4
N_o(cm^{-3})	2.65×10^{17}	1.82×10^{15}	2.22×10^{17}	1.60×10^{16}	2.65×10^{17}

N (10^{19} cm^{-3})	**2.1**	**3.3**	**4.4**	**4.6**	**12**
Present J_{Eo}-results are obtained, using Equations (44, 9)					
$g_c = 6, n_i = 1.07 \times 10^{10}$ cm^{-3}					
P(N, W)<<1	5.7×10^{-5}	2.2×10^{-4}	7.2×10^{-5}	1.7×10^{-4}	6.6×10^{-5}
$\frac{\tau_{t,eff.}}{\tau_h(N)} \ll 1$	1.6×10^{-9}	2.4×10^{-8}	2.6×10^{-9}	1.4×10^{-8}	2.2×10^{-9}
Present $J_{Eo}(S \to \infty)$	3.242×10^{-12}	8.448×10^{-13}	2.554×10^{-12}	1.080×10^{-12}	2.774×10^{-12}
RD(%)	-1.32	-1.78	1.77	1.78	0.94
$g_c = 5, n_i = 9.77 \times 10^{9}$ cm^{-3}					
P(N, W)<<1	5.0×10^{-5}	1.9×10^{-4}	6.1×10^{-5}	1.4×10^{-4}	5.7×10^{-5}
$\frac{\tau_{t,eff.}}{\tau_h(N)} \ll 1$	1.2×10^{-9}	1.8×10^{-8}	1.9×10^{-9}	1.0×10^{-8}	1.6×10^{-9}
Present $J_{Eo}(S \to \infty)$	3.054×10^{-12}	8.124×10^{-13}	2.485×10^{-12}	1.052×10^{-12}	2.693×10^{-12}
RD(%)	4.56	2.12	4.43	4.35	3.81
$g_c = 4.9113, n_i = 9.68 \times 10^{9}$ cm^{-3}					
P(N, W)<<1	4.9×10^{-5}	1.8×10^{-4}	6.1×10^{-5}	1.4×10^{-4}	5.6×10^{-5}
$\frac{\tau_{t,eff.}}{\tau_h(N)} \ll 1$	1.2×10^{-9}	1.7×10^{-8}	1.8×10^{-9}	1.0×10^{-8}	1.6×10^{-9}
J_{Eo} (A/cm^2)	3.038×10^{-12}	8.096×10^{-13}	2.479×10^{-12}	1.050×10^{-12}	2.686×10^{-12}
RD(%)	5.07	2.46	4.66	4.57	4.07
Present J_{Eo}-results are obtained, using Equations (44, 15)					
$g_c = 6, n_i = 1.07 \times 10^{10}$ cm^{-3}					
P(N, W)<<1	5.7×10^{-5}	2.2×10^{-4}	7.2×10^{-5}	1.7×10^{-4}	6.5×10^{-5}
$\frac{\tau_{t,eff.}}{\tau_h(N)} \ll 1$	1.6×10^{-9}	2.3×10^{-8}	2.6×10^{-9}	1.5×10^{-8}	2.1×10^{-9}
Present $J_{Eo}(S \to \infty)$	3.277×10^{-12}	8.472×10^{-13}	2.543×10^{-12}	1.073×10^{-12}	2.813×10^{-12}
RD(%)	-2.41	-2.07	2.20	2.42	-0.48
$g_c = 5, n_i = 9.77 \times 10^{9}$ cm^{-3}					
P(N, W)<<1	5.0×10^{-5}	1.9×10^{-4}	6.2×10^{-5}	1.5×10^{-4}	5.4×10^{-5}
$\frac{\tau_{t,eff.}}{\tau_h(N)} \ll 1$	1.2×10^{-9}	1.8×10^{-8}	1.9×10^{-9}	1.1×10^{-8}	1.5×10^{-9}
Present $J_{Eo}(S \to \infty)$	3.083×10^{-12}	8.107×10^{-13}	2.460×10^{-12}	1.040×10^{-12}	2.808×10^{-12}
RD(%)	3.66	2.32	5.37	5.49	-0.30
$g_c = 4.9113, n_i = 9.68 \times 10^{9}$ cm^{-3}					
P(N, W)<<1	4.9×10^{-5}	1.9×10^{-4}	6.1×10^{-5}	1.4×10^{-4}	5.3×10^{-5}
$\frac{\tau_{t,eff.}}{\tau_h(N)} \ll 1$	1.2×10^{-9}	1.7×10^{-8}	1.9×10^{-9}	1.0×10^{-8}	1.4×10^{-9}
Present $J_{Eo}(S \to \infty)$	3.066×10^{-12}	8.075×10^{-13}	2.453×10^{-12}	1.037×10^{-12}	2.809×10^{-12}
RD(%)	4.20	2.71	5.64	5.75	-0.31

The underlined $|RD|$-values are the maximal ones.

Table 4 indicates that:

(i) the maximal relative deviations (RDs) in absolute values between our results (44, 9) and the J_{Eo}-data [10, 12] are found to be: 1.78% for g_c=6, 4.56% for g_c=5, and 5.07% for g_c=4.9113, and

(ii) the maximal RDs in absolute values between our results (44, 15) and the J_{Eo}-data [10, 12] are given by: 2.42% for g_c=6, 5.49% for g_c=5, and 5.75% for g_c=4.9113. It suggests that our numerical results (44, 9) for g_c=6 are the best ones, since they are accurate within 1.78%. Further, one notes that our ΔE_{ga}-expression given in Equation (9) was obtained, taking into account all the physical effects such as: those of donor size, heavy doping and Fermi-Dirac statistics, while in Equation (15) our $\Delta E_{ga(Mod.YC)}$ -expression is only an empirical one. So, in the following, we will choose: g_c=6, T=300 K, and our ABGN-expression (9), for all the numerical calculations.

(iii) Furthermore, in particular, for large S and small P, from Equation (40) one gets:

$$\frac{J_{Eo}(x=0,N,r_d,S)}{J_{Eo}(x=W,N,r_d,S)} = \frac{1}{\cosh(P)+I\times\sinh(P)} \simeq 1 - \frac{D_h(N_o(W))}{S\times L_h(N_o(W))} \times P - \frac{(P)^2}{2}.$$

Then, from Equation (43), using Equations (20, 37) one obtains in the heavily doped case:

$$\tau_{t,eff.}(x = W, N, r_d, g_c, S) \simeq \tau_h \times \left\{\frac{D_h(N_o(W))}{S \times L_h(N_o(W))} \times P + \frac{(P)^2}{2}\right\} \simeq \frac{W}{S} \times \frac{L_h(N_o(W))}{L_{h,eff.}(N_o(W))} + \frac{W^2}{2D_h(N_o(W))} \times \left(\frac{L_h(N_o(W))}{L_{h,eff.}(N_o(W))}\right)^2$$

$$\simeq \frac{W^2}{2D_h(N_o(W))} \times \left(\frac{L_h(N_o(W))}{L_{h,eff.}(N_o(W))}\right)^2, \text{as } S \to \infty \quad (45)$$

and in the lowly doped case (i.e., $L_{h,eff.} \simeq L_h$):

$$\tau_{t,eff.}(x = W, N, r_d, S) \equiv \tau_t = \frac{W}{S} + \frac{W^2}{2D_h} \simeq \frac{W^2}{2D_h}, \text{as } S \to \infty \quad (46)$$

being just a familiar expression given for the minority-hole transit time τ_t obtained by Shibib et al. [7].

5.2. Small $S = 10^{-50}$ $(\frac{cm}{s})$ or $S \to 0$, and $P \gg 1$ or $W \gg L_{h,eff}$

Here, from Eq. (33) and for any N, one has: I =

$\frac{D_h(N_o(W))}{S\times L_h(N_o(W))} \to \infty$, since $S \to 0$. Therefore, from Equation (43), one obtains: $\frac{\tau_{t,eff.}(x=W\gg L_{h,eff.},N,r_d,g_c,S\to 0)}{\tau_h} \to 1$, suggesting a completely opaque emitter region (COER).

Now, our numerical results of $J_{Eo}(x = W, N, r_d, S) \equiv J_{Eo}$ and $\frac{\tau_{t,eff.}(x=W,N,r_d,S)}{\tau_h} \equiv \frac{\tau_{t,eff.}}{\tau_h}$, for simplicity, are respectively computed, using Equations (39) and (43), and then plotted into Figures 3 (a_1, a_2), (b) and 4 (a_1, a_2), (b) as functions of N, and Figures 3 (c) and 4 (c), as functions of S, noting that in those figures we also include various physical conditions such as: S, W, r_d and N.

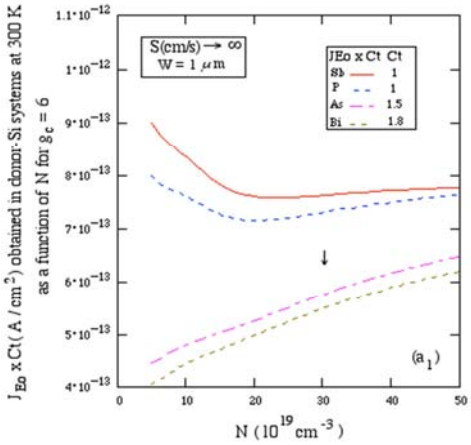

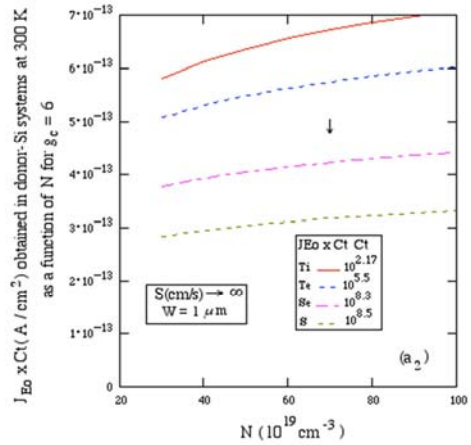

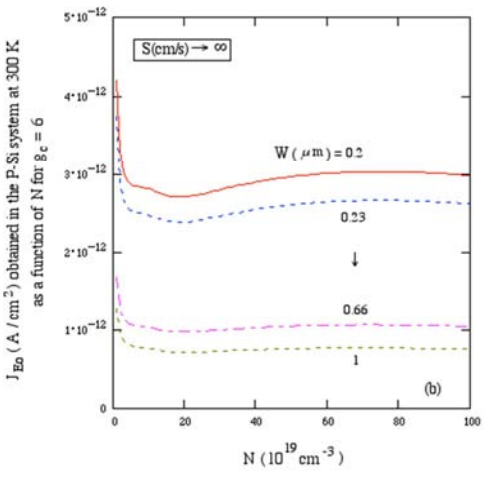

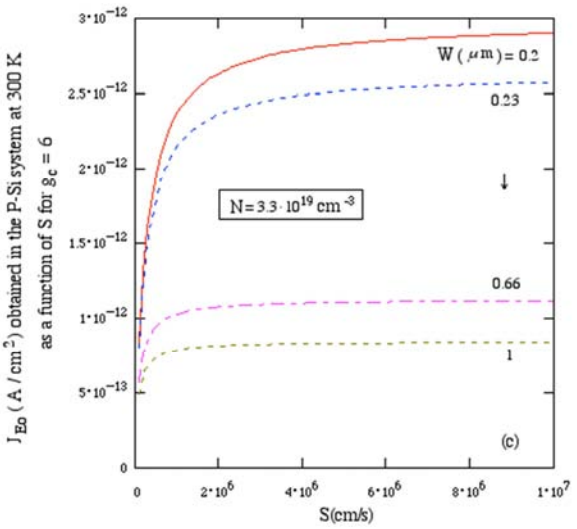

Figure 3. *(a_1, a_2) Our J_{Eo}-results obtained as functions of N, with a condition: $N > N_{cn}(r_d)$, given in heavily doped donor-Si systems, as defined in Table 1, (b) ours obtained as a function of N, and (c) ours obtained as a function of S.*

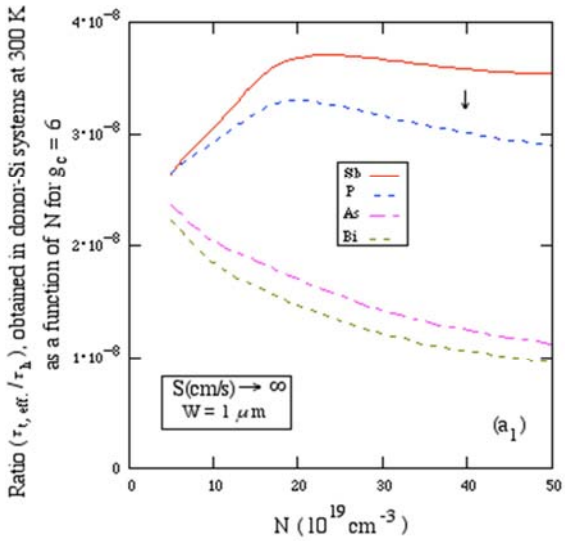

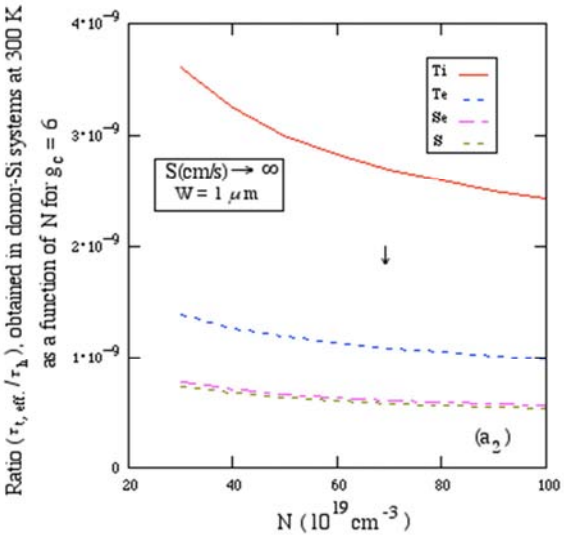

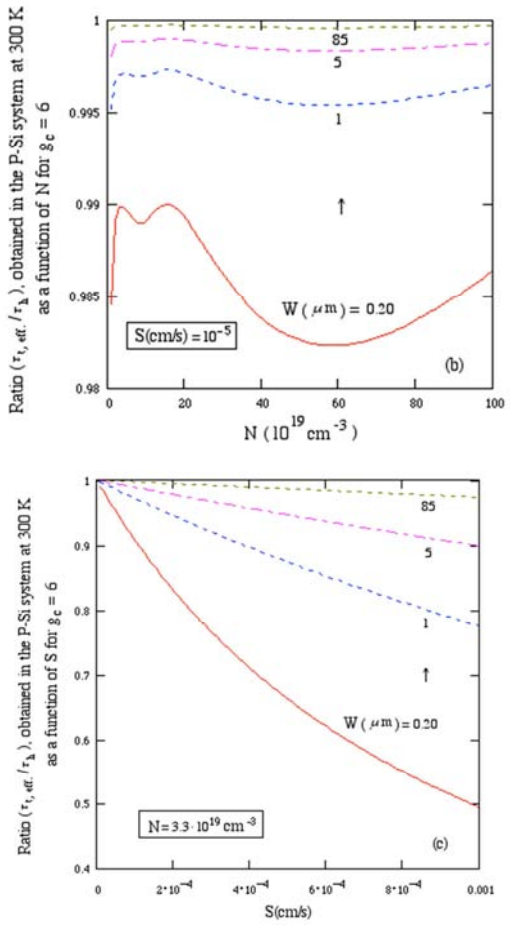

Figure 4. *(a_1, a_2) Our ($\tau_{t,eff.}/\tau_h$)-results obtained as functions of $N > N_{cn}(r_d)$ in heavily doped donor-Si systems, as defined in Table 1, (b) ours obtained as a function of N, and (c) ours obtained as a function of S.*

Some concluding remarks are obtained and discussed below.

(i) Figures 3(a_1, a_2) and 4(a_1, a_2) indicate that, since as $S \to \infty$ and $W = 1\ \mu m$, $\frac{\tau_{t,eff.}}{\tau_h} (< 4 \times 10^{-8}) \simeq 0$, according to the CTER, and for a given N, due to the donor-size effect, both J_{Eo} and $\frac{\tau_{t,eff.}}{\tau_h}$ decrease (↓) with increasing r_d. Then, for a given r_d, at large values of $N \geq 3 \times 10^{20}$ cm^{-3}, due to the heavy doping effect, J_{Eo} (or $\frac{\tau_{t,eff.}}{\tau_h}$) increases (or decreases) with increasing N.

(ii) Figures 3(b) and 4(b) show that, for a given N, J_{Eo} (or $\frac{\tau_{t,eff.}}{\tau_h}$) decreases (or increases) with increasing W.

(iii) Figures 3(c) and 4(c), suggest that, for given S, J_{Eo} (or $\frac{\tau_{t,eff.}}{\tau_h}$) decreases (or increases) with increasing W.

(iv) In particular, in Figure 4(c), as $S \to 0$ and $W = 85\ \mu m$, $\frac{\tau_{t,eff.}}{\tau_h} \to 1$, according to the COER.

Finally, it should be noted that in next Section 6 we must know the numerical results of dark saturation current density, defined by:

$$J_o(x = W, N, r_d, S, N_a, r_a) \equiv J_{Eo}(x = W, N, r_d, S) + J_{Bo}(N_a, r_a) \quad (47)$$

where J_{Bo} and J_{Eo} are determined respectively in Equations (21, 39). Then, those are tabulated in the following Table 5, in which all the physical conditions are also presented.

Table 5. *Our numerical results of $J_o = J_{Eo} + J_{Bo}$, calculated using Equation (47), where J_{Bo} and J_{Bo} are determined respectively in Equations (21, 39), and those are obtained in the three following cases.*

First case: In the heavily doped (HD) P-Si emitter region ($N = 10^{20}$ cm^{-3}), and in the lightly doped (LD) B-Si base region ($N_a = 10^{16}$ cm^{-3}) in which $J_{Bo} = 6.0912 \times 10^{-13}\ \left(\frac{A}{cm^2}\right)$.

For $S = 10^{50}$ cm/s and $W = 0.206$ nm, according to the completely transparent emitter region, one has:

$J_{Eo} = 2.4833 \times 10^{-9}\ \left(\frac{A}{cm^2}\right) \gg J_{Bo}$ and $J_o = 2.4839 \times 10^{-9}\ \left(\frac{A}{cm^2}\right) \simeq J_{Eo}$

For $S = 10^{50}$ cm/s and $W = 4.4$ nm, according also to the completely transparent emitter region, one has: $J_{Eo} = 1.1645 \times 10^{-10}\ \left(\frac{A}{cm^2}\right) \gg J_{Bo}$ and $J_o = 1.1706 \times 10^{-10}\ \left(\frac{A}{cm^2}\right) \simeq J_{Eo}$

For $S = 10^4$ cm/s and $W = 0.36$ μm, one has: $J_{Eo} = 1.2237 \times 10^{-13}\ \left(\frac{A}{cm^2}\right) < J_{Bo}$ and $J_o = 7.3148 \times 10^{-13}\ \left(\frac{A}{cm^2}\right) \simeq J_{Bo}$

For $S = 10^{-50}$ cm/s and $W = 85$ μm, according also to the completely opaque emitter region, one has: $J_{Eo} = 4.7117 \times 10^{-19}\ \left(\frac{A}{cm^2}\right) \ll J_{Bo}$ and $J_o = 6.0912 \times 10^{-13}\ \left(\frac{A}{cm^2}\right) = J_{Bo}$

Second case: In the completely opaque HD S-Si emitter region ($N = 5 \times 10^{20}$ cm^{-3}, $S = 10^{-50}$ cm/s and $W = 85$ μm), and in the lightly doped a-Si base region, in which $N_a = 10^{16}$ cm^{-3}.

(r_S, r_a)	(r_S, r_B)	(r_S, r_{Al})	(r_S, r_{Ga})	(r_S, r_{In})	(r_S, r_{Tl})
$J_{Eo}\ \left(\frac{A}{cm^2}\right)$	1.8728×10^{-29}	1.8728×10^{-29}	1.8728×10^{-29}	1.8728×10^{-29}	1.8728×10^{-29}
$J_{Bo}\ \left(\frac{A}{cm^2}\right)$	6.0912×10^{-13}	1.8033×10^{-13}	1.3660×10^{-13}	2.6485×10^{-15}	5.3080×10^{-17}
$J_o\ \left(\frac{A}{cm^2}\right)$	6.0912×10^{-13}	1.8033×10^{-13}	1.3660×10^{-13}	2.6485×10^{-15}	5.3080×10^{-17}

$J_o = J_{Bo}$

Third case: In the completely transparent HD d-Si emitter region ($N = 5 \times 10^{20}$ cm^{-3}, $S = 10^{50}$ cm/s and $W = 0.000206$ μm), and in the lightly doped Tl-Si base region, in which $N_a = 10^{16}$ cm^{-3} and $J_{Bo} = 5.3080 \times 10^{-17}\ \left(\frac{A}{cm^2}\right)$.

(r_d, r_{Tl})	(r_{Sb}, r_{Tl})	(r_P, r_{Tl})	(r_{As}, r_{Tl})	(r_{Bi}, r_{Tl})
$J_{Eo}\ \left(\frac{A}{cm^2}\right)$	2.7206×10^{-9}	2.6794×10^{-9}	1.5402×10^{-9}	1.2336×10^{-9}
$J_o\ \left(\frac{A}{cm^2}\right)$	2.7206×10^{-9}	2.6794×10^{-9}	1.5402×10^{-9}	1.2336×10^{-9}

(r_d, r_{Tl})	(r_{Ti}, r_{Tl})	(r_{Te}, r_{Tl})	(r_{Se}, r_{Tl})	(r_S, r_{Tl})
$J_{Eo}\left(\frac{A}{cm^2}\right)$	1.6600×10^{-11}	7.5378×10^{-15}	9.7654×10^{-18}	4.6878×10^{-18}
$J_o\left(\frac{A}{cm^2}\right)$	1.6600×10^{-11}	7.5909×10^{-15}	6.2845×10^{-17}	$5.7767 \times 10^{-17} \simeq J_{Bo}$

Some important remarks are given and discussed below.

(i) In the first case, with decreasing S and increasing W, J_o thus decreases from the CTER to the COER, and one gets in this COER: $J_o = J_{Bo}$.

(ii) In the second case or in the COER-conditions, J_{Bo} decreases with increasing r_a, being due to the acceptor-size effect, and for given r_a one has: $J_o = J_{Bo}$ since $J_{Eo} = 0$.

(iii) In the third case or in the CTER-conditions, J_{Eo} decreases with increasing r_d, being due to the donor-size effect, and for (r_S, r_{Tl}), one gets: $J_o = 5.7767 \times 10^{-17}\left(\frac{A}{cm^2}\right) \simeq J_{Bo} = 5.3080 \times 10^{-17}\left(\frac{A}{cm^2}\right)$, which can be compared with the similar result, obtained the second case or in the COER-conditions, as: $J_o = J_{Bo} = 5.3080 \times 10^{-17}\left(\frac{A}{cm^2}\right)$, calculated for (r_S, r_{Tl}).

It should be noted that these values of J_o will strongly affect the variations of various photovoltaic conversion parameters of $n^+ - p$ junction silicon solar cells, such as: the ideality factor n, short circuit current density J_{sc}, fill factor FF, and photovoltaic conversion efficiency η, being expressed as functions of the open circuit voltage, V_{oc} [4], as investigated in the following. Our empirical treatment method used is that of two points. The first point is characterized by [27]:

$$V_{oc1} = 624 \text{ mV},\ J_{sc1} = 36.3\ \frac{mA}{cm^2}, FF_1 = 80.1\ \% \quad (48)$$

and the second one by [23, 28]:

$$V_{oc2} = 740 \text{ mV}, J_{sc2} = 41.8\ \frac{mA}{cm^2}, FF_2 = 82.7\ \%. \quad (49)$$

In the following, we will develop our empirical treatment method of two points, used to determine J_{sc} and FF, basing on accurate results given in Equations (48) and (49).

6. Photovoltaic Conversion Effect

The well-known net current density J at T=300 K, expressed as a function of the applied voltage V, flowing through the $n^+ - p$ junction of silicon solar cells, is defined by:

$$J(V) \equiv J_{ph.}(V) - J_o \times \left(e^{\frac{V}{n(V)\times V_T}} - 1\right), V_T \equiv \frac{k_B T}{e} = 25.8543 \text{ mV} \quad (50)$$

Noting that $J(V) = 0$ at $V = V_{oc}$, V_{oc} being an open circuit voltage, at which $J_{ph.}(V = V_{oc}) \equiv J_{sc}(W, N, r_d, S, N_a, r_a, V_{oc})$, where J_{sc} is the short circuit current density. Here, $J_{ph.}$ is the photocurrent density and $J_o(W, N, r_d, S, N_a, r_a) \equiv J_{Eo} + J_{Bo}$ is the "dark saturation current density" or the $n^+ - p$ junction leakage saturation current density in the absence of light, defined in Equation (47). Therefore, the photovoltaic conversion effect occurs, according to:

$$J_{sc}(W, N, r_d, S, N_a, r_a, V_{oc}) \equiv J_o(W, N, r_d, S, N_a, r_a) \times (e^v - 1), v(W, N, r_d, S, N_a, r_a, V_{oc}) \equiv \frac{V_{oc}}{n \times V_T} \quad (51)$$

Here, n is the ideality factor, being determined by our empirical treatment method of two points, as:

$$n(W, N, r_d, S, N_a, r_a, V_{oc}) = n_1(W, N, r_d, S, N_a, r_a, V_{oc1}, J_{sc1}) + n_2(W, N, r_d, S, N_a, r_a, V_{oc2}, J_{sc2}) \times \left(\frac{V_{oc}}{V_{oc1}} - 1\right)^{y_n},$$

$$y_n = 1.1248 \quad (52)$$

which is valid for any $W, N, r_d, S, N_a, r_a, V_{oc} \geq V_{oc1}$, and increases with increasing V_{oc} for given W, N, r_d, S, N_a and r_a.

Further, the values of V_{oc1}, J_{sc1}, V_{oc2} and J_{sc2} are given in Equations (48, 49), and the numerical results of $n_{1(2)}$ can be determined from Equation (51) by:

$$n_{1(2)}(W, N, r_d, S, N_a, r_a, V_{oc1(2)}, J_{sc1(2)}) \equiv \frac{V_{oc1(2)}}{V_T} \times \frac{1}{\ln\left(\frac{J_{sc1(2)}}{J_o} + 1\right)} \quad (53)$$

implying that both $n_{1(2)}$ (or n) and J_o have the same variations for given (W, N, r_d, S, N_a, r_a)-variations, being found to be an important remark.

Furthermore, in Equation (52), for the CTER-conditions such as:

$$W = 4.4 \text{ nm} = 0.0044\ \mu m, N = 10^{20}\ cm^{-3}, r_d = r_P, S = 10^{50}\ \frac{cm}{s}, N_a = 10^{16}\ cm^{-3}, r_a = r_B \quad (54)$$

the exponent $y_n = 1.1248$ was chosen such that:

$$n(W, N, r_d, S, N_a, r_a, V_{oc1(2)}) \equiv n_{1(2)}(W, N, r_d, S, N_a, r_a, V_{oc1(2)}, J_{sc1(2)}) = 1.2344\ (1.4534) \text{ respectively.}$$

For example, from the above remark given in Eq. (53) and from the first case reported in Table V, we can conclude that, with decreasing S and increasing W, both n and J_o decrease from the CTER to the COER. Therefore, from Equation (51), J_{sc} thus increases from the CTER to the COER, since J_{sc} is expressed in terms of $e^{v\equiv\frac{V_{oc}}{n\times V_T}}$.

Then, the values of the fill factor FF for $V_{oc} = V_{oc1(2)}$ can be found to be given by:

$$FF_{1(2)}\left(W, N, r_d, S, N_a, r_a, V_{oc1(2)}\right) = \frac{v(W,N,r_d,S,N_a,r_a,V_{oc1(2)}) - \ln[v(W,N,r_d,S,N_a,r_a,V_{oc1(2)}) + 0.72]}{v(W,N,r_d,S,N_a,r_a,V_{oc1(2)}) + z_{FF_{1(2)}}} \quad (55)$$

where $z_{FF_{1(2)}} = 1.1\ (0.472)$ was chosen such that, under the above conditions (54), the values of $FF_{1(2)}$, calculated using Equation (55), are identical to the data given in Equations (48, 49): 80.1% (82.7%), respectively [27, 23].

Moreover, in the case where both series resistance and shunt resistance have a negligible effect upon cell performance, $z_{FF_{1(2),Green}} = 1$, as proposed by Green [4].

Now, by applying a same above treatment method of two points, one has:

$$FF(W, N, r_d, S, N_a, r_a, V_{oc}) = FF_1(W, N, r_d, S, N_a, r_a, V_{oc1}) + FF_2(W, N, r_d, S, N_a, r_a, V_{oc2}) \times \left(\frac{V_{oc}}{V_{oc1}} - 1\right)^{y_{FF}},$$

$$y_{FF} = 2.0559 \quad (56)$$

which is valid for any $W, N, r_d, S, N_a, r_a, V_{oc} \geq V_{oc1}$, and increases with increasing V_{oc} for given W, N, r_d, S, N_a and r_a. Here, the value of $y_{FF}(= 2.0559)$ was chosen such that, under the conditions (54), $FF\left(W, N, r_d, S, N_a, r_a, V_{oc1(2)}\right) \equiv FF_{1(2)}\left(W, N, r_d, S, N_a, r_a, V_{oc1(2)}\right) = 80.1\%\ (82.7\%)$, respectively [27, 23].

Then, the photovoltaic conversion efficiency η can be defined by:

$$\eta(W, N, r_d, S, N_a, r_a, V_{oc}) \equiv \frac{J_{sc}\times V_{oc}\times FF}{P_{in.}} \quad (57)$$

where J_{sc} and FF are determined respectively in Equations (51, 56), being assumed to be obtained at 1 sun illumination or at AM1.5G spectrum $(P_{in.} = 0.100\ \frac{W}{cm^2})$ [27, 28].

In summary, all above parameters such as: n, J_{sc}, FF and η, defined in above, strongly depend on J_o, determined in Equation (47), which is thus a central result of the present paper.

Now, for given physical conditions such as: W, N, r_d, S, N_a and r_a, and by taking into account all remarks given in Table 5 and also in above Equation (53), our numerical results of n, J_{sc}, FF and η, expressed as functions V_{oc}, are respectively computed by using Equations (52, 51, 56, 57), and reported in following Table 6 and Figures 7, 8 and 9.

In Table 6, in which, for $624 \leq V_{oc}(mV) \leq 750$ [23, 24, 27-29] the physical conditions used are:

$$W = 0.206\ nm, N = 10^{20}\ cm^{-3}, r_d \equiv r_P, S = 10^{50}\ \frac{cm}{s}, N_a = 10^{16}\ cm^{-3}, r_a \equiv r_B \quad (58)$$

according to the CTER, we get the precisions of the order of 8.1% for J_{sc}, 7.1% for FF, and 5% for η, calculated using the corresponding data [23, 24, 27-29], which is strongly affected by $J_o = J_{Eo} + J_{Bo}$, as noted above, suggesting thus an accuracy of J_{Bo} $(\leq 8.1\%)$, since J_{Eo} was accurate within 1.78%, as given in Table 4.

Table 6. *With the physical conditions given in Equation (58), our present results (PR) of n, $J_{sc}(\frac{mA}{cm^2})$, FF(%), and $\eta(\%)$, calculated using Equations (52,51,56,57), being compared with corresponding data [23, 24, 27-29], and their relative deviations (RD), computed using the formula: RD=$|1-(PR/Data)|$.*

Data (D) from References	V_{oc} (mV)	n	$J_{sc(PR)}\left(J_{sc(D)}\right)$; RD	$FF_{(PR)}\left(FF_{(D)}\right)$; RD	$\eta_{(PR)}\left(\eta_{(D)}\right)$; RD
[28]	750	1.7474	40.24 (39.5); 1.9	80.58 (83.2); 3.1	24.32 (24.7); 1.5
[23, 28]	740	1.7222	41.01 (41.8); 1.9	80.11 (82.7); 3.1	24.31 (25.6); 5.0
[28]	738	1.7172	41.16 (40.8); 0.9	80.02 (83.5); 4.2	24.31 (25.1); 3.2
[28]	737	1.7146	41.23 (41.3); 0.2	80.00 (82.7); 3.3	24.30 (25.2); 3.6
[28]	718	1.6676	42.43 (42.1); 0.8	79.22 (83.2); 4.8	24.13 (25.1); 3.8
[24]	710	1.6481	42.82 (42.3); 1.2	78.95 (82.6); 4.4	24.00 (24.8); 3.2
[28, 29]	706	1.6384	42.98 (42.7); 0.6	78.82 (82.8); 4.8	23.91 (25.0); 4.3
[24]	705	1.6360	43.02 (42.2); 1.9	77.87 (83.1); 6.3	23.89 (24.7); 3.3
[24]	703	1.6312	43.08 (42.0); 2.6	78.73 (82.7); 4.8	23.84 (24.4); 2.3
[28]	695	1.6122	43.30 (40.2); 7.7	78.50 (80.5); 2.5	23.62 (22.5); 4.9
[28]	680	1.5772	43.37 (40.5); 7.1	78.14 (80.3); 2.7	23.05 (22.1); 4.3
[29]	671.7	1.5584	43.20 (40.5); 6.5	77.98 (80.9); 3.6	22.63 (22.0); 2.8
[28]	667	1.5479	43.01 (39.8); 8.1	77.91 (80.0); 2.6	22.35 (21.3); 4.9
[27]	665	1.5434	43.91 (42.2); 1.7	76.87 (78.7); 1.0	22.22 (22.1); 0.5

Data (D) from References	V_{oc} (mV)	n	$J_{sc(PR)}(J_{sc(D)})$; RD	$FF_{(PR)}(FF_{(D)})$; RD	$\eta_{(PR)}(\eta_{(D)})$; RD
[24]	655	1.5217	42.21 (39.8); 6.1	77.74 (79.4); 2.1	21.50 (20.7); 3.8
[28]	643	1.4968	40.83 (39.3); 3.9	77.64 (83.6); 7.1	20.38 (21.1); 3.4
[27]	632	1.4758	38.80 (39.2); 1.0	77.59 (75.8); 2.4	19.02 (18.7); 1.7
[27]	624	1.4630	36.30 (36.3); 0.0	77.58 (80.1); 3.1	17.57 (18.1); 2.9

The underlined RD (%)-values are the maximal ones.

In Figures 5 (a), (b), (c) and (d), the physical conditions used are:

$$N = 10^{20}\ cm^{-3}, r_d = r_P, N_a = 10^{16}\ cm^{-3}, r_a = r_B, \text{and different } (S, W) - \text{values} \quad (59)$$

which are given also in these figures, and in Table 5 for the first case. Here, for a given V_{oc}, and with decreasing S and increasing W, we observe that:

(i) in the Figure 5 (a), the function n determined in Equation (52) (or the function J_o given in Table 5) decreases from the CTER to the COER

(ii) in Figures 5 (b), 5 (c) and 5(d), the functions J_{sc}, FF and η therefore increase from the CTER to the COER, and

(iii) in Figure 5 (d), for the physical functions: W=85 μm and $S = 10^{-50}$ cm/s, the function η reaches a maximum equal to 27.77% at V_{oc}=715 mV; here $1\ \mu m = 10^{-6}$ m.

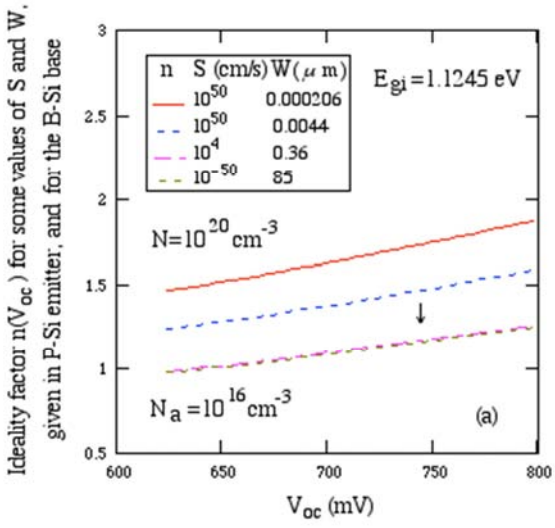

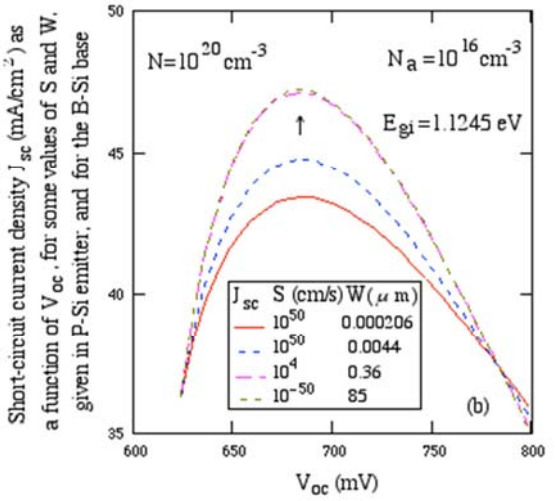

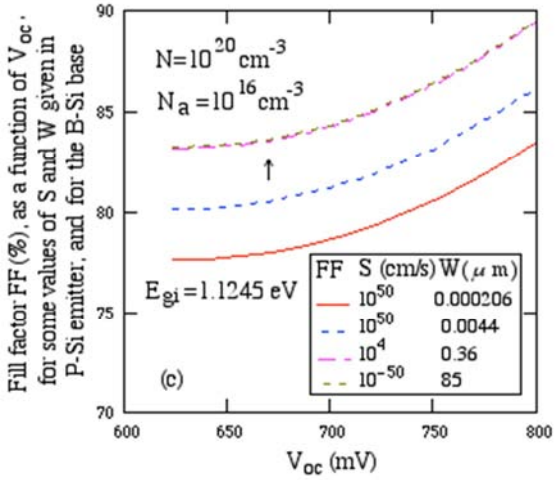

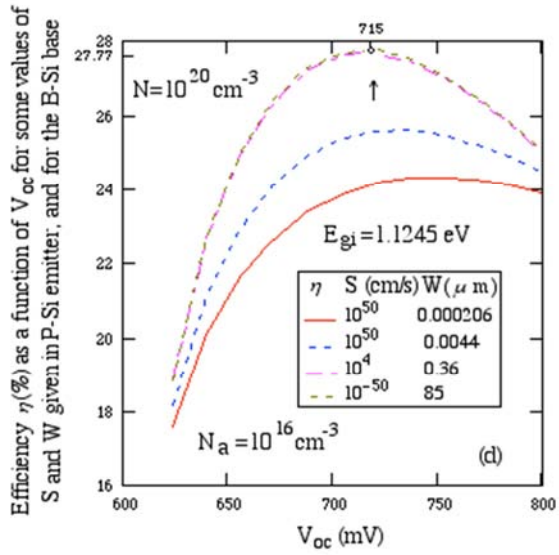

Figure 5. *(a) Our n-results, (b) $J_{sc}(\frac{mA}{cm^2})$-results, (c) FF(%)-results, and (d) η(%)-results, plotted as functions of V_{oc} and obtained with increasing W and decreasing S (or from the completely transparent emitter region to the completely opaque emitter region).*

In Figures 6 (a), (b), (c) and (d), the physical conditions used are:

$$W = 85\ \mu m, N = 5 \times 10^{20}\ cm^{-3}, r_d = r_S, S = 10^{-50}\frac{cm}{s},$$
$$N_a = 10^{16}\ cm^{-3}, r_a, \text{and } E_{gi}(r_a) \text{ at } 300\ K \quad (60)$$

according to the COER, and they are also given in these

figures and in Table 5 for the second limiting case, in which $J_o = J_{Bo}$, since $J_{Eo} = 0$. Thus, this simplifies the numerical calculation of functions n, J_{sc}, FF and η, using Equations (52, 51, 56, 57), where J_o is replaced by J_{Bo}, determined by Eq. (21). Further, in Equation (60), the values of $E_{gi}(r_a)$ are given in Table 2. Then, for a given V_{oc} and with increasing r_a-values, it should be concluded that, due to the acceptor-size effect,

(i) in the Figure 6 (a), the function n determined in Equation (52) (or the function J_o given in Table 5) decreases (↓), and

(ii) in Figures 6 (b), (c), (d), the functions J_{sc}, FF and η therefore increase (↑), and in particular, in Figure 6 (d), for the completely opaque (S-Si) emitter-region conditions, where J_{Eo}=0 or J_o=J_{Bo}, the maximal η-values are equal to: 27.77 %,…, 31.55 %, at V_{oc}=715 mV,…,703 mV, according to the E_{gi}-values equal to: 1.12 eV,…, 1.34 eV, which are obtained in various lightly doped (B,…, Tl)-Si base regions, respectively, being due to the acceptor-size effect.

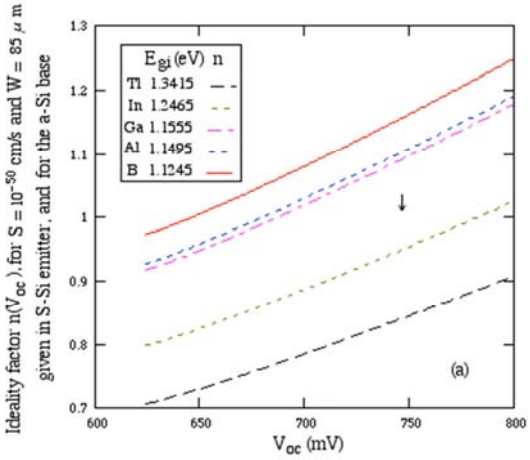

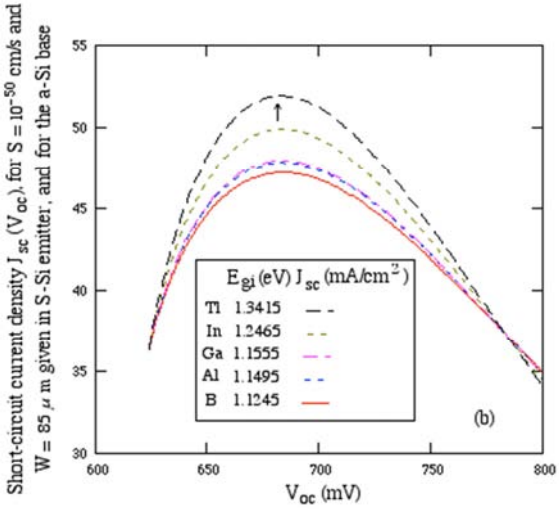

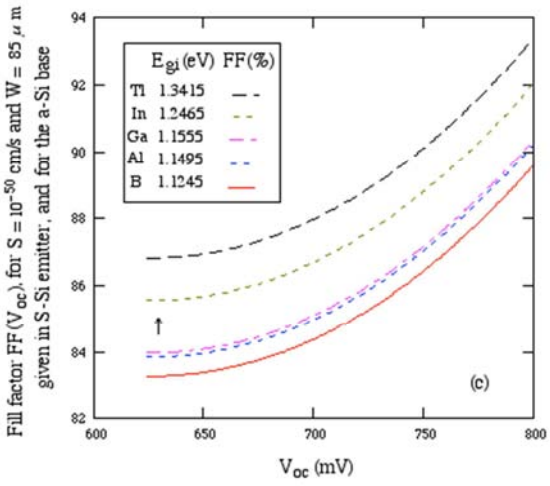

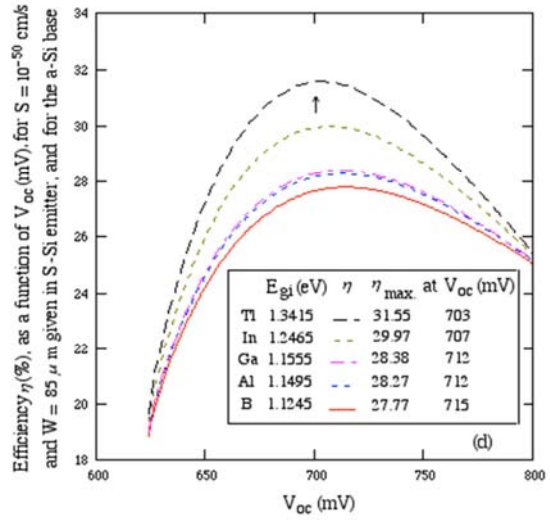

Figure 6. *For $N = 5 \times 10^{20}\ cm^{-3}$ and $N_a = 10^{16}\ cm^{-3}$, (a) our n-results, (b) $J_{sc}(\frac{mA}{cm^2})$-results, (c) FF(%)-results, and (d) η(%)- results, plotted as functions of V_{oc} and obtained in the COER-conditions.*

Finally, in Figures 7 (a), (b), (c) and (d), the physical conditions used are:

$$W = 0.000206\ \mu m, N = 5 \times 10^{20}\ cm^{-3}, r_d, S = 10^{50}\ \frac{cm}{s},$$

$$N_a = 10^{16}\ cm^{-3}, r_{Tl}, \text{and } E_{gi}(r_d) \text{ at } 300\ K \qquad (61)$$

according to the CTER, and they are also given in Table 5 for the third case. Here, the values of $E_{gi}(r_d)$ at 300 K are given in Table 2. Then, the numerical results of n, J_{sc}, FF and η are calculated, using Equations (52, 51, 56, 57). Further, for a given V_{oc} and with increasing r_a -values, it should be concluded that, due to the donor-size effect,

(i) in the Figure 7 (a), the function n determined in Equation (52) (or the function J_o given in Table 5) decreases (↓), and

(ii) in Figures 7 (b), (c), (d), the functions J_{sc}, FF and η therefore increase (↑), and in particular, in Figure 7 (d), in the conditions of completely transparent and heavily doped (donor-Si) emitter-and- lightly doped (Tl-Si) base regions, the maximal η-values are equal to:

24.28 %,…, 31.51 %, at V_{oc} =748 mV,…,703 mV, according to the E_{gi}-values equal to: 1.11 eV,…, 1.70 eV, obtained in various (Sb,…, S)-Si emitter regions, respectively, being due to the donor-size effect, which can be compared with those given in Figure 6 (d).

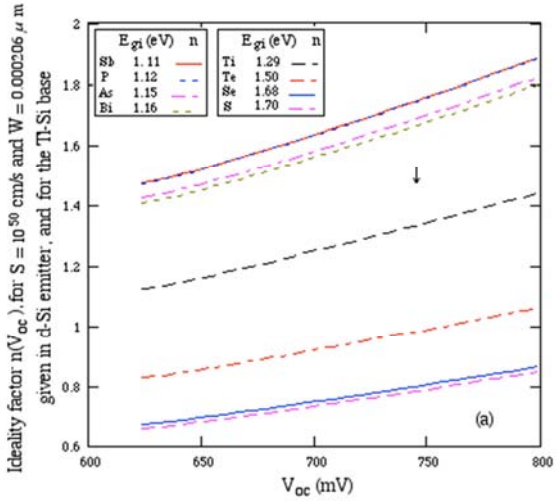

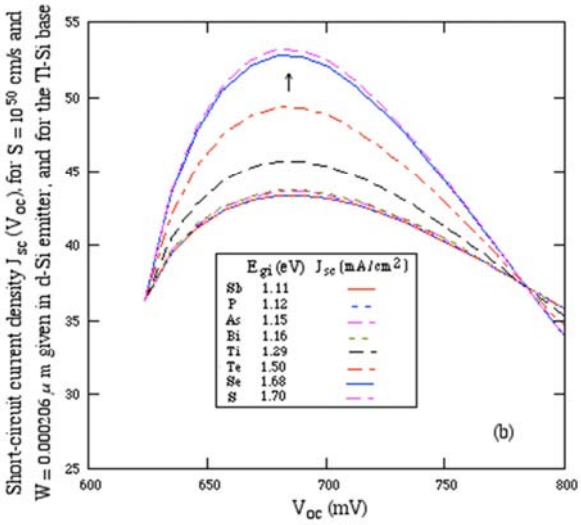

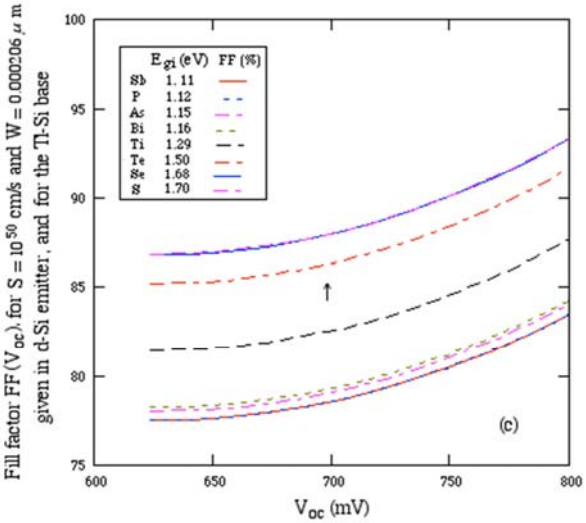

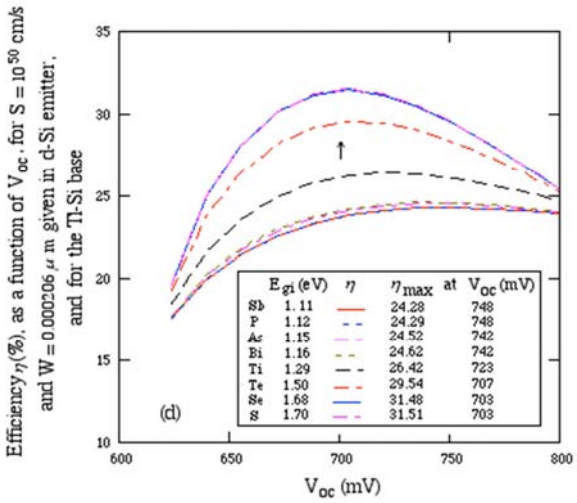

Figure 7. *For $N = 5 \times 10^{20}\ cm^{-3}$ and $N_a = 10^{16}\ cm^{-3}$, (a) our n-results, (b) $J_{sc}(\frac{mA}{cm^2})$-results, (c) FF(%)-results, and (d) η(%)- results, plotted as functions of V_{oc} and obtained in the CTER-conditions.*

7. Concluding Remarks

We have developed the effects of heavy doping and impurity size on various parameters at 300 K, characteristic of energy-band structure, as given in Sections 2 and 3, and of the performance of crystalline silicon solar cells, being strongly affected by the dark saturation current density: $J_o \equiv J_{Eo} + J_{Bo}$, as given in Sections 4, 5 and 6. Then, some concluding remarks are obtained and discussed as follows.

1 Using the OPG (E_{g1})-data given by Wagner and del Alamo [44], our E_{g1}-results, due to the heavy doping effect, and calculated using Equation (16), are found to be accurate within 1.86%, as observed in Table 3.

2 In the CTER-conditions, as those given in Table 4, and using the J_{Eo}-data, given by del Alamo et al. [10, 12], by using Equation (44), our J_{Eo}-results, obtained in the heavily doped and completely transparent (P-Si) emitter region, are found to be accurate within 1.78%, while the modeled J_{Eo} -results, obtained by those authors, are accurate within 36% [10, 12].

3 For given physical conditions and using an empirical treatment method of two points, as developed and discussed in Section 6, both our two results (n and J_o) have the same variations, which strongly affect other (V_{oc}, J_{sc}, FF, η)-results, as discussed in Eq. (53). Thus, J_o, determined in Equation (47), is a central result of our present paper.

4 In the CTER-conditions, as those given in Equation (58), and using various (J_{sc}, FF, η)-data [23, 24, 27-29], we get the precisions of the order of 8.1% for J_{sc}, 7.1% for FF and 5% for η, suggesting thus a probable accuracy of J_{Bo} ($\leq 8.1\%$), since our J_{Eo} -results are accurate within 1.78%.

5 In the physical conditions of completely opaque and heavily doped (S-Si) emitter-and-lightly doped (acceptor-Si) base regions, as given in Eq. (60), and in the physical conditions of completely transparent and heavily doped (donor-Si) emitter-and-lightly doped (Tl-

Si) base regions, as given in Eq. (61), our obtained maximal η-values, due to the impurity-size effect, are found to be equal respectively to: 27.77%, …, 31.55%, as seen in Figure 6 (d), and 24.28%, …, 31.51%, as observed in Figure 7 (d), suggesting that our obtained highest η-values are found to be almost equal, as: $31.51\% \simeq 31.55\%$, since the two corresponding limiting J_o-values are almost the same, as given in Table 5, for second and third cases.

In summary, being due to the impurity-size effects, our limiting value of η_1=31.55%, as that given in Figure 6 (d), is thus obtained in the following limiting physical conditions as:

$$W = 85\ \mu m, N = 5 \times 10^{20}\ cm^{-3}, E_{gi}(r_d = r_S) = 1.7035\ eV, S = 10^{-50}\frac{cm}{s},$$

$$N_a = 10^{16}\ cm^{-3}, \text{and } E_{gi}(r_a = r_{Tl}) = 1.3415, \text{at } 300\ K,$$

and η_2=27.77%, as that given in Figure 5 (d), is obtained in the following limiting physical conditions as:

$$W = 85\ \mu m, N = 10^{20}\ cm^{-3}, E_{gi}(r_d = r_P) = 1.1245\ eV, S = 10^{-50}\frac{cm}{s},$$

$$N_a = 10^{16}\ cm^{-3}, \text{and } E_{gi}(r_a = r_B) = 1.1245, \text{at } 300\ K.$$

Those limiting $\eta_{1,2}$–results can be compared with that obtained by Richter et al. (R) [26], η_R=29.43%, for a thick 100 μm solar cell made of un-doped silicon, as: $\eta_2 < \eta_R < \eta_1$.

Acknowledgments: We thank Prof. Dr. Nghi Q. Lam, the Former Editor-in-Chief of Applied Physics Letters (1994-2014), for his helpful remarks and suggestions, which have greatly improved the presentation of our paper.

Appendix

Appendix A: Fermi Energy

The Fermi energy E_F, obtained for any T and donor density N, being investigated in our previous paper, with a precision of the order of 2.11×10^{-4} [39], is now summarized in the following. First of all, we define the reduced electron density by:

$$u(N, T, r_d, g_c) \equiv \frac{N}{N_c(T, r_d, g_c)} \equiv \mathcal{F}_{1/2}(\theta) \quad (A1)$$

where N_c is defined in Eq. (6), $\theta(u) \equiv \frac{E_F(u)}{k_B T}$ is the reduced Fermi energy, and $\mathcal{F}_{1/2}(\theta)$ is the Fermi-Dirac integral, defined by [40]:

$$\mathcal{F}_{\frac{1}{2}}(\theta) \equiv \frac{2}{\sqrt{\pi}}\int_0^\infty \frac{x^{\frac{1}{2}}dx}{1+e^{x-\theta}}, x \equiv \frac{E}{k_B T} \quad (A2)$$

which was calculated for any values of θ, with a precision of the order of 10^{-7}, by Van Cong and Doan Khanh [40], using a theorem existence of Hermite interpolating polynomials. Then, by a reversion method of $u \equiv \mathcal{F}_{1/2}(\theta)$ so useful to obtain $\theta(u)$, concerned with doped semiconductors at arbitrary N and T, our expression for reduced Fermi energy was found to be given by [39]:

$$\theta(u) \equiv \frac{E_F(u)}{k_B T} = \frac{G(u)+Au^B F(u)}{1+Au^B}, \text{with } A = 0.0005372 \text{ and } B = 4.82842262 \quad (A3)$$

where, in the degenerate case or when $\theta(u \gg 1) \to \infty$, Equation (A3) is reduced to:

$F(u) = au^{\frac{2}{3}}\left(1 + bu^{-\frac{4}{3}} + cu^{-\frac{8}{3}}\right)^{-\frac{2}{3}}$; $a = \left[3\sqrt{\pi}/4\right]^{2/3}$, $b = \frac{1}{8}\left(\frac{\pi}{a}\right)^2$, and $c = \frac{62.3739855}{1920}\left(\frac{\pi}{a}\right)^4$, and in the non-degenerate case or when $\theta(u \ll 1) \ll 0$, to:

$$G(u) \simeq Ln(u) + 2^{-\frac{3}{2}} \times u \times e^{-du}, d = 2^{3/2}\left[\frac{1}{\sqrt{27}} - \frac{3}{16}\right] > 0$$

Appendix B: Approximate Form for Band Gap Narrowing (BGN)

First of all, we will normalize the various energies by using the effective Rydberg energy R, as:

$$R(T, r_d) = 13.605693 \times \frac{m_c(T, r_d)}{\varepsilon^2(r_d)}(eV) \quad (A4)$$

and we express the effective Wigner-Seitz radius r_s characteristic of the interactions by:

$$r_s(N, T, r_d, g_c) \equiv \left(\frac{3g_c}{4\pi N}\right)^{\frac{1}{3}} \times \frac{1}{a_B(T, r_d)}$$

Here, $a_B(T, r_d) = 5.2917715 \times 10^{-9} \times \frac{\varepsilon(r_d)}{m_c(T, r_d)}$ (cm) is the Bohr radius. Therefore, one has:

$$r_s(N, T, r_d, g_c) = 1.1723 \times 10^8 \times \left(\frac{g_c}{N}\right)^{1/3} \times \frac{m_c(T, r_d)}{\varepsilon(r_d)} \quad (A5)$$

Therefore, the ratio R/r_s is thus proportional to: $\frac{\varepsilon(r_P)}{\varepsilon(r_d)} \times N_r^{1/3}$, where $N_r \equiv \left(\frac{6 \times N}{g_c \times 9.999 \times 10^{17}\ cm^{-3}}\right)$. Now, an empirical expression for BGN is proposed by:

$$\Delta E_g(N, T, r_d, g_c) = \equiv -R \times \mu_{XE}(r_s) - R \times \mu_c(r_s) - R \times \mu_n^{h-Cor}(r_s) - R \times \mu_n^{e-d}(r_s) - R \times \mu_n^{h-d}(r_s) + \Delta E_{g(LT)} \quad (A6)$$

where, R and r_s are defined above, and five first contributions of the spin-polarized chemical potential energy μ were determined in our previous paper [42], and sixth μ-one by Lanyon and Tuft [6]. One notes here that the second $-R \times \mu_c(r_s)$-term of Equation (A6) represents the shift in majority conduction-band edge, due to the correlation (Cor) energy of an effective electron gas, $E_c(r_s)$, as [42]:

$$E_c(N, T, r_d, g_c) = \frac{-0.87553}{0.0908+r_s} + \frac{\frac{0.87553}{0.0908+r_s} + \left(\frac{2[1-\ln(2)]}{\pi^2}\right) \times \ln(r_s) - 0.093288}{1+0.03847728 \times r_s^{1.67378876}} \quad (A7)$$

and that from the a Seitz's theorem [42], one has:

$$\mu_c(N,T,r_d,g_c) \equiv \frac{-r_s^4}{3} \times \frac{\partial}{\partial r_s}\frac{E_c(r_s)}{r_s^3} = -E_c(r_s) + \frac{r_s}{3} \times \frac{\partial}{\partial r_s}E_c(r_s) \simeq 2.503 \times [-E_c(r_s)] \equiv \mu_{c(A)}(r_s), \quad (A8)$$

being obtained with an accuracy of 1.87% for $g_c = 6$ in various donor-Si systems. Then, an approximate expression for the BGN is found to be given by:

$$\Delta E_g(N,T,r_d,g_c) \simeq a_1 \times \frac{\varepsilon(r_P)}{\varepsilon(r_d)} \times N_r^{1/3} + a_2 \times \frac{\varepsilon(r_P)}{\varepsilon(r_d)} \times N_r^{\frac{1}{3}} \times (2.503 \times [-E_c(r_s) \times r_s]) + a_3 \times \left[\frac{\varepsilon(r_P)}{\varepsilon(r_d)}\right]^{5/4} \times \left[\frac{m_c(T,r_d)}{m_c(T,r_P)}\right]^{1/4} \times N_r^{1/4} \times \sqrt{\frac{m_v(T)}{m_c(T,r_d)}} + a_4 \times \sqrt{\frac{m_c(T,r_P)\times\varepsilon(r_P)}{m_c(T,r_d)\times\varepsilon(r_d)}} \times N_r^{1/2} \times \left\{1 + \sqrt{\frac{m_c(T,r_d)}{m_c(T,r_P)}}\right\} + a_5 \times \left[\frac{m_c(T,r_d)}{m_c(T,r_P)}\right]^{1/2} \times \left[\frac{\varepsilon(r_P)}{\varepsilon(r_d)}\right]^{\frac{3}{2}} \times N_r^{\frac{1}{6}} \quad (A9)$$

noting that, in the P-Si system for 300 K, these constants: $a_1 = 3.8 \times 10^{-3}$ (eV), $a_2 = 6.5 \times 10^{-4}$ (eV), $a_3 = 2.8 \times 10^{-3}$ (eV), $a_4 = 5.597 \times 10^{-3}$ (eV), and $a_5 = 8.1 \times 10^{-4}$ (eV), were chosen such that for $g_c = 6$ the numerical results of minority-carrier saturation current J_{Eo} are found to be accurate within 1.78%, as seen in Table 4.

References

[1] F. A. Lindholm, A. Neugroschel, C. T. Sah, M. P. Godlewski, and H. W. Brandhorst, "A methodology for experimentally based determination of gap shrinkage and effective lifetimes in the emitter and base of p-n junction solar cells and other p-n junction devices," IEEE Trans. Electron Devices ED, vol. 24, pp. 402-410, 1977.

[2] W. Shockley and H. J. Queisser, " Detailed balance limit of efficiency of p-n junction solar cells." J. Appl. Phys., vol. 32, pp. 510-519, 1961.

[3] J. W. Slotboom, H. C. de Graaff, "Measurements of band gap narrowing in Si bipolar transistors," Solid-State Electron., vol. 19, pp. 857-862, 1976.

[4] M. A. Green, "Solar cell fill factors: general graph and empirical expressions," Solid-State Electron., vol. 24, pp. 788-789, 1981.

[5] R. M. Swanson and R. A. Sinton," Advances in Solar Energy," edited by K. A. Bouer, American Solar Energy, Newark, Delaware, 1990.

[6] H. Van Cong and S. Brunet, "Effective drift current densities in the n-type heavily doped emitter region of p - n^+ junction silicon solar cells, "Solar Cells," vol. 5, pp. 355-365, 1982.

[7] M. A. Shibib, F. A. Lindholm, and F. Therez, "Heavily doped transparent-emitter region in junction solar cells, diodes, and transistors," IEEE Trans. Electron Devices, vol. ED-26, pp. 959-965, 1979.

[8] J. del Alamo and R. M. Swanson, "The physics and modeling of heavily doped emitters," IEEE Trans. Electron Devices, vol. ED-31, pp. 1878-1888, 1984.

[9] R. A. Logan, J. F. Gilbert, and F. A. Trumbore, "Electron mobilities and tunneling currents in silicon, "J. Appl. Phys.," vol. 32, pp. 131-132, 1961.

[10] J. del Alamo, S. Swirhum, and R. M. Swanson, "Measuring and modeling minority carrier transport in heavily doped silicon, "Solid-State Electron.," vol. 28, pp. 47-54, 1985.

[11] D. Chattopadhyay and H. J. Queisser, "Electron scattering by ionized impurities in semiconductors," Rev. Mod. Phys., vol. 53, pp. 745-768, 1981.

[12] R. M. Swanson, "Modeling of minority-carrier transport in heavily doped silicon emitters, "Solid-State Electron.," vol. 30, pp. 1127-1136, 1987.

[13] Z. Essa, N. Taleb, B. Sermage, C. Broussillon, B. Bazer-Bachi, and M. Quillec, "Doping profile measurement on textured silicon surface," EPJ Photovoltaics, vol. 9, p. 5, 2018.

[14] S. C. Jain, E. L. Heasell, and D. J. Roulston, "Recent advances in the physics of silicon p-n junction solar cells including their transient response," Prog. Quant. Electron., vol. 11, pp. 105-204, 1987.

[15] S. C. Jain and D. J. Roulston, "A simple expression for band gap narrowing in heavily doped Si, Ge, GaAs and Ge_XSi_{1-X} strained layers," Solid-State Electron., vol. 34, pp. 453-465, 1991.

[16] D. B. M. Klaassen, J. W. Slotboom, and H. C. de Graaff, "Unified apparent band gap narrowing in n- and p-type silicon," Solid-State Electron., vol. 35, pp. 125-129, 1992.

[17] A. Zouari, A. B. Arab, "A simple formulation of the saturation current density in heavily doped emitters," Can. J. Phys., vol. 81, pp. 1109-1120, 2003.

[18] N. Stem and M. Cid, "Studies of phosphorus Gaussian profile emitter silicon solar cells," Materials Research, vol. 4, pp. 143-152, 2001.

[19] D. Yan and A. Cuevas, "Empirical determination of the energy band gap narrowing in highly doped n^+ silicon," J. Appl. Phys., vol. 114, p. 044508, 2013.

[20] F. H. Alharbi and S. Kais, "Theoretical limits of photovoltaics efficiency and possible improvements by intuitive approaches learned from photosynthesis and quantum coherence, "Renewable and sustainable energy reviews," vol. 43, pp. 1073-1089, 2015.

[21] A. Cuevas, J. G. Fossum, and R. T. Young, "Influence of the dopant density profile on minority-carrier current in shallow, heavily doped emitters of silicon bipolar devices," Solid-State Electron., vol. 28, pp. 247-254, 1985.

[22] H. Van Cong, "A simple accurate solution to minority electron injection in the p-type heavily doped emitter region of silicon devices," Physica Status Solidi A, Vol. 149, pp. 619-628, 1995.

[23] K. Masuko, M. Shigematsu, T. Hashiguchi, D. Fujishima, M. Kai, N. Yoshimura, T. Yamaguchi, Y. Ichihashi, T. Mishima, N. Matsubara, T. Yamanishi, T. Takahama, M. Taguchi, E. Maruyama, and S. Okamoto, "Achievement of more than 25% conversion efficiency with crystalline silicon heterojunction solar cell," IEEE J. Photovoltaic, vol. 4, pp. 1433-1435, 2014.

[24] A. Fell, K. R. McIntosh, P. P. Altermatt, G. J. M. Janssen, R. Stangl, A. Ho-Baillie, H. Steinkemper, J. Greulich, M. Müller, B. Min, K. C. Fong, M. Hermle, I. G. Romijn, and M. D. Abbott, "Input Parameters for the simulation of silicon solar cells in 2014," IEEE J. Photovoltaics, vol. 5, pp. 1250-1263, 2015.

[25] H. Van Cong, "A new solution for minority-carrier injection into the heavily doped emitter of silicon devices," Physica Status Solidi A, vol. 171, pp. 631-645, 1999.

[26] A. Richter, M. Hermle, and S. W. Glunz, " Reassessment of the limiting efficiency for crystalline silicon solar cells," IEEE J. Photovoltaics, vol. 3, pp. 1184-1191, 2013.

[27] R. S. Davidsen, H. Li, A. To, X. Wang, A. Han, J. An, J. Colwell, C. Chan, A. Wenham, M. S. Schmidt, A. Boisen, O. Hansen, S. Wenham, and A. Barnett, "Black silicon laser-doped selective emitter solar cell with 18.1% efficiency," Sol. Energy Mater. Sol. Cells," vol. 144, pp. 740-747, 2016.

[28] C. Battaglia, A. Cuevas, and S. De Wolf, "High-efficiency crystalline silicon solar cells: status and perspectives, "Energy Environ. Sci., vol. 9, pp. 1552-1576, 2016.

[29] M. A. Green, Y. Hishikawa, E. D. Dunlop, D. H. Levi, J. Hohl-Ebinger, and A. W. Y. Ho-Baillie, "Solar cell efficiency tables (version 51)," Prog. Photovolt. Res. Appl., vol. 26, pp. 3-12, 2018.

[30] J. E. Lang, F. L. Madarasz, and P. M. Hemenger, "Temperature dependent density of states effective mass in non-parabolic p-type silicon," J. Appl. Phys., vol. 54, pp. 3612-3612, 1983.

[31] M. A. Green, "Intrinsic concentration, effective densities of states, and effective mass in silicon," J. Appl. Phys., vol. 67, pp. 2944-2954, 1990.

[32] H. Van Cong, "Band gap changes in excited intrinsic (heavily doped) Si and Ge semiconductors," Physica B, vol. 405, pp. 1139-1149, 2010.

[33] R. Pässler, "Dispersion-related description of temperature dependencies of band gaps in semiconductors," Phys. Rev. B, vol. 66, p. 085201, 2002.

[34] R. Pässler, "Semi-empirical descriptions of temperature dependences of band gaps in semiconductors," Physica Status Solidi B, vol. 236, pp. 710-728, 2003.

[35] O. Henri-Rousseau and P. Blaise, Quantum Oscillators, edited by John Wiley & Sons, Inc., Hoboken, New Jersey, 2011.

[36] A. B. Sproul and M. A. Green, "Improved value for the silicon intrinsic carrier concentration from 275 to 375 K," J. Appl. Phys., vol. 70, pp. 846-854, 1991.

[37] K. Misiakos and D. Tsamakis, "Accurate measurements of the silicon intrinsic carrier density from 77 to 340 K," J. Appl. Phys., vol. 74, pp. 3293-3297, 1993.

[38] R. Couderc, M. Amara, and M. Lemiti, "Reassessment of the intrinsic carrier density temperature dependence in crystalline silicon," J. Appl. Phys., vol. 115, p. 093705, 2014.

[39] H. Van Cong and G. Debiais, "A simple accurate expression of the reduced Fermi energy for any reduced carrier density," J. Appl. Phys., vol. 73, pp. 1545-15463, 1993.

[40] H. Van Cong and B. Doan Khanh, "Simple accurate general expression of the Fermi-Dirac integral Fi(a) for arbitrary a and j> -1," Solid-State Electron., vol. 35, pp. 949-951, 1992.

[41] H. Van Cong, S. Abide, B. Zeghmati, and X. Chesneau, "Optical band gap in various impurity-Si systems from the metal-insulator transition study," Physica B, vol. 436, pp. 130-139, 2014.

[42] H. Van Cong, "Effects of impurity size and heavy doping on energy-band-structure parameters of various impurity-Si systems," Physica B, vol. 487, pp. 90-101, 2016.

[43] H. Van Cong, "Effects of donor size and heavy doping on optical, electrical and thermoelectric properties of various degenerate donor-silicon systems at low temperatures," American Journal of Modern Physics, vol. 7, pp. 136-165, 2018.

[44] J. Wagner and J. A. del Alamo, "Band-gap narrowing in heavily doped silicon: A comparison of optical and electrical data," J. Appl. Phys., vol. 63, pp. 425-429, 1988.

[45] H. Van Cong, "Fermi energy and band-tail parameters in heavily doped semiconductors," J. Phys. Chem. Solids, vol. 36, pp. 1237-1240, 1975.